Evaluation of the impact of charge/discharge profiles on SIBs ageing

Francisco Ramos da Silva
Master in Engineering Physics
Department of Physics and Astronomy
Faculty of Sciences of University of Porto
Faculty of Engineering of University of Porto
2025

Evaluation of the impact of charge/discharge profiles on SIBs ageing

Francisco Ramos da Silva

Internship Report carried out as part of the
Master in Engineering Physics

Department of Physics and Astronomy

2025

Supervisor
Dr. Miguel Duarte, PhD Researcher, Faculty of Engineering of University of Porto

External Host Supervisor
Dr. Rita Carvalho Veloso, Electrochemistry Team Leader, Vasco da Gama CoLab

Acknowledgements

I would like to begin by thanking my supervisors, Dr. Miguel Duarte and Dr. Rita Carvalho Veloso, whose contribution and guidance throughout the development of this thesis was essential for all stages of the developed work. I would also like to thank Vasco da Gama CoLab for providing the opportunity, materials and help to carry out the experimental part of this work.

A very special acknowledgment and appreciation to my family, for supporting and providing me with all the care, assistance and tools necessary for my academic success.

I would also like to deeply thank all of my friends that accompanied me throughout my six years completing this course, in particular to Raquel Pereira, who always supported and believed in me, and João Lopes, who faced this academic journey with me.

Resumo

Num mundo com avanços tecnológicos cada vez maiores, a dependência em energia elétrica é cada vez mais fundamental para a sociedade, criando, naturalmente, a necessidade de dispositivos para armazenar essa energia. A bateria de ião de lítio (LIB) foi rapidamente adotada como a principal opção de armazenamento de energia, devido à sua elevada potência, capacidade e densidade energética. O uso de LIBs começou a ser questionado com a disponibilidade limitada de lítio na crosta da Terra, despertando a procura por alternativas viáveis e com maior disponibilidade. Investigação extensiva concluiu a bateria de ião sódio (SIB) como um ótimo substituto, dadas as semelhanças com as de lítio em termos de composição, o que facilitaria a transição entre tecnologias. O desempenho eletroquímico das SIBs também é bastante notável, com um grande desafio no maior raio iónico do sódio, que reduz significativamente a densidade energética possível numa única célula. No entanto, investigação nesta alternativa merece atenção para aplicações estacionárias, onde o tamanho da bateria não será tão restritivo.

O estudo sobre a degradação e o envelhecimento das baterias é vital para compreender melhor como a sua vida útil pode ser prolongada ao máximo possível. Embora este tópico já esteja muito desenvolvido no que diz respeito às LIBs, no que toca às SIBs, sendo uma alternativa mais recente, ainda carecem de literatura sobre o seu envelhecimento.

Este trabalho tem como objetivo analisar o envelhecimento cíclico de 28 SIBs comerciais de formato 18650 e os seus mecanismos de degradação, a fim de melhorar o conhecimento sobre esta tecnologia. Estas células foram submetidas a vários protocolos de carga/descarga diferentes.

Esta análise foi feita com o estudo da evolução de várias métricas eletroquímicas ao longo dos ciclos, tais como capacidade de armazenamento de energia, corrente elétrica, tensão, eficiência coulômbica e capacidade diferencial. Também será realizada uma espectroscopia de impedância eletroquímica post mortem nestas baterias, para fornecer uma melhor compreensão das suas alterações internas. Uma caracterização inicial das baterias com a ajuda da capacidade diferencial concluiu que elas são compostas por um cátodo de análogo do azul da prússia ($Na_{2-x}FeFe(CN)_6$) à base de ferro e um ânodo de *hard carbon*.

Neste trabalho, vários protocolos foram desenvolvidos, de modo a serem avaliados vários fatores pela sua comparação: taxa de corrente elétrica, janela de estado de carga (

SoC), perfis em pulso e carregamento a tensão constante. Foi estabelecida uma relação entre um maior crescimento da *solid electrolyte interface* (SEI) e uma taxa de corrente elétrica mais elevada, sendo o protocolo de taxa 1C considerado o melhor em termos de degradação da bateria. Os protocolos de janelas SoC mostraram valores elevados de impedância interna e revelaram-se bastante destrutivos para os elétrodos, uma vez que as condições limitadas impediram-nos de completar totalmente a suas transições de fase adequadamente. Os perfis em pulso revelaram-se conservadores, proporcionando tempos de carga mais rápidos, mas com retenção de capacidade semelhante ao protocolo com melhores resultados. Quanto à etapa de tensão constante, verificou-se que conduzia a uma degradação total dos materiais dos elétrodos, uma vez que a inserção/-remoção total dos iões de sódio criou tensões mecânicas e deformações adicionais na sua estrutura.

Palavras-chave: baterias de ião sódio, bateris de ião lítio, envelhecimento cíclico, mecanismos de degradação, análogos do azul da prússia, hard carbon, estado de carga, taxa de corrente, carga em pulsos

Abstract

In a world with more technological advancements each passing day, reliance on electrical energy is fundamental to society, naturally creating the need for devices to store electrical energy. The lithium-ion battery (LIB) was quickly adopted as the leading energy storage option, for its high power, capacity and energy density. LIBs usage started raising issues with a limited lithium availability in the Earth's crust, sparking desire to find viable alternatives with more availability. Research indicates the sodium-ion battery (SIB) as a great replacement, given the similarities with their lithium counterparts in composition, the transition between technologies would be facilitated. The performance of SIBs is quite remarkable as well, with a major challenge being the bigger ionic size of sodium, as it greatly reduces the energy density possible in a single cell, yet their research still warrants attention for stationary applications, where size isn't a big constraint.

Research into battery degradation and aging is vital to better understand how the lifetime can be prolonged as much as possible. While this topic is already very developed when it comes to LIBs, their sodium counterparts, being a somewhat more recently looked into alternative, still lack in literature about aging. This study aims to analyse the cyclic aging of 28 commercial 18650 format SIBs and their degradation mechanisms in order to improve the knowledge into this technology. These cells were submitted to several different charge/discharge profiles to evaluate their impact on degradation. This evaluation was done with the study of the evolution of several electrochemical metrics through the cycles, such as capacity, electrical current, voltage, coulombic efficiency (CE) and differential capacity. Post-mortem electrochemical impedance spectroscopy (EIS) will also be performed on these batteries, to provide better insight into their inner changes. An initial characterization of the batteries with the help of differential capacity concluded they are composed of an iron-based prussian blue analogue cathode ($Na_{2-x}FeFe(CN)_6$) and a hard carbon anode.

This work developed several protocols meant to draw comparisons between them and evaluate the impact of certain factors: current C-rate, state of charge (SoC) window, pulse profiles and constant voltage charging. A relation between bigger solid electrolyte interface (SEI) growth and higher C-rate was drawn, as the 1C C-rate protocol was found to be the best in terms of battery degradation. The SoC windows protocols showed high values of internal impedance and revealed to be quite destructive on the electrodes, as the limited conditions impeded their phase transitions to properly complete. The pulse profiles

proved to be conservative, providing faster charge times yet similar capacity retention to the best resulting protocol. As for the constant voltage step, it proved to lead to a total degradation of the electrode materials, as the much more complete insertion/removal of sodium ions created additional stress and strain in their structure.

Keywords: sodium-ion batteries, lithium-ion batteries, cyclic aging, degradation mechanisms, prussian blue analogues, hard carbon, state of charge, C-rate, pulse charging

Table of Contents

List of Figures

List of Tables

List of Abbreviations

CC constant current. 14

CE coulombic efficiency. iv, 8

CPE constant phase element. 12

EIS electrochemical impedance spectroscopy. iv, 9

HC hard carbon. 5

JT Jahn-Teller. 10

LAM loss of active material. 2

LIB lithium-ion battery. ii, iv, 1

LSI loss of sodium inventory. 2

NMR Na-solid state nuclear magnetic resonance. 17

OCV open circuit voltage. 23

PBA prussian blue analogue. 6

PCC pulse charge charge. 15

PCD pulse charge discharge. 15

PCR pulse charge rest. 15

PMR P-solid state nuclear magnetic resonance. 17

SEI solid electrolyte interface. iii, iv, 2

SEM scanning electron microscopy. 14

SIB sodium-ion battery. ii, iv, 1

SoC state of charge. iii, iv, 2

SoH state of health. 7

XRD X-ray diffraction. 14

1. Introduction

1.1. Background

So much of our modern world and technology is dependent on electricity, yet most of its production is centred around fossil fuels, such as coal, natural gas and oil [1]. These resources are a major topic of contention given their polluting nature, threatening the deterioration of our environment, and given they are finite, raising questions of their viability in the extremely long term. As a way of preventing these less than desirable effects, the development and exploration of renewable and environmentally sustainable energy production, through methods like solar and wind, has garnered worldwide attention. These technologies, however, are somewhat unreliable and lack consistency due to their dependence on external factors, such as the weather, which leads to periods of over and underproduction. Therefore, large scale energy storage devices are a promising solution [2]. Even in the smaller scale, these technologies are extremely useful and important for devices now considered essential such as mobile phones and personal computers [3].

In the last few decades, the type of batteries that have garnered more attention and development have been the lithium-ion battery (LIB), due to their long service life and excellent energy storage and density [4]. Lithium, however, comes with its problems, namely in its cost and extraction. It's not overly abundant in the Earth's crust, therefore most of the Li reserves currently being explored are concentrated in a few countries, and other methods of extraction like with ocean water are very costly and complicated to implement [5]. Furthermore, Lithium is a very reactive element and thus cannot be paired with common metals like Copper or Aluminium in its electrodes, usually opting for elements like Cobalt. This raises further problems, as the biggest Cobalt reserve in the world is found in the Democratic Republic of Congo and is surrounded by several ethical and human rights controversies [6]. In order to avoid these problems, in search of better sustainability and cheaper options, alternatives to LIBs are widely researched. A very promising and recently explored technology are the sodium-ion battery (SIB), which were discovered around the same time as LIBs but were outclassed early by discoveries and breakthroughs in the latter.

In the recent decade, more and more cathode and anode materials are being developed for SIBs, leading to great promise and progress as reliable batteries. There are also

advantages in the similarities the two elements share, as the already implemented processes and techniques for creating both types of batteries are similar, allowing for a good transition between the technologies [7]. Sodium-ion batteries avoid some of the problems raised by their Lithium counterparts, as it is a much more abundant element in the Earth's crust and is not reactive to common metals such as Iron, Copper, Aluminium and Manganese, offering much cheaper and easier to obtain electrode materials [8]. Even further, SIBs present lower thermal runway risk and dendrite growth in its cells, given the generally better stability of sodium. Even with its advantages and advancements in research, there are still flaws to be noted in these batteries. One example is the lower energy density when compared to LIBs, indicating less favourability to smaller, more portable uses. A major point of contention that warrants study and research is the battery service life. Especially from a consumer point of view, an electronic device isn't considered of much quality if its battery is in frequent need of repairment or replacement. Even from a sustainable point of view, having to frequently fabricate new batteries and dispose of old ones is just creating more waste and general pollution. With intensive use, certain side reactions occur within a cell and lead to a fade in capacity leading the battery to hold less charge and thus being discharged faster with each use. This is what is referred to as aging, and it is divided into two types: calendar aging and cycle aging. The former deals with the degradation suffered with the battery being stored without any use, losing capacity over time. The latter, which is the focus of this project, is about the capacity fade resulting from the use and charge/discharge cycling of the cell. This study is focused on exploring the degradation mechanisms that lead to this aging, and to better understand what triggers them and which factors have any effect on their development. From an overall literature review, the most common mechanisms seem to be excessive or irregular solid electrolyte interface (SEI) formation, loss of active material (LAM) through electrode cracking and destruction, loss of sodium inventory (LSI) through parasitic side reactions such as sodium plating, phase transition in the electrodes and reduced ion mobility.

1.2. Objectives and Overview

The aim of this work is to test several 18650 commercial SIBs in several cycling protocols with varying current rate, voltage limits, state of charge (SoC) window, pulse charges and other varying elements, to study the effect these factors have on the aging of this technology. The evolution of the battery parameters will be analysed to fully understand the electrochemical and physical mechanisms that lead to the degradation of the cells. Key weaknesses of sodium-ion batteries will be highlighted, for any possible future study.

Furthermore, there are the added objectives of better formulating protocols that can avoid and protect the battery against certain forms of degradation, as well as forming better knowledge on what factors cause more aggressive degradation on SIBs.

1.3. Thesis Outline

This thesis is organized in 5 chapters. Chapter 1, Introduction, is to present the subject that will be studied, as well as providing the motivation and objective of this work. Chapter 2, Background and State of the Art, dives into the ion battery technology that we will be working with, it's current state in research, and their biggest problems and challenges. Chapter 3, Experimental Methods, will present the materials and devices this work will be utilizing as well as provide an outline for the experimental protocols performed. Chapter 4, Results and Discussion, presents the resulting data, plots and curves from the experimental procedures, providing an initial characterization of our studied batteries and an analysis on how each protocol affected the overall aging. Chapter 5, Conclusions and Future work, will summarize the findings of this work and expand on what could be improved or used for future research related to the topic.

2. Background and State of the Art

2.1. Fundamentals of Rechargeable Ion Batteries

Batteries are electrochemical energy storage devices, storing and releasing energy through electrochemical reactions. These reactions take place in a cell, composed of two electrodes, one positive (cathode) and one negative (anode), and an electrolyte. The batteries tackled in this study are rechargeable ion batteries, sometimes referred to as rocking chair batteries, where specific ions are intercalated within the electrodes in a reversible process. The positive electrode is composed of a material containing the main ion component, generally presenting crystal structures with vacancies where these ions can be inserted and stored. The preferred cathode materials can withstand this insertion and subsequent removal of ions in a way that does not compromise the overall structure and stability of the component. These factors are key features for the anodes as well, who also suffer the insertion/removal of ions. The main electrochemical process in a battery are the redox reactions activated in the electrodes to maintain balance with the movement of the ions, thus providing a flow of both ions and electrons. Given the reversibility in this process, the electrodes themselves are either positive or negative depending on if it is a charge or a discharge, but for convenience and simplicity, conventionally the cathode is the one where reduction occurs in the discharge, whereas the anode is where the oxidation occurs.

During the energy discharge, there is a spontaneous flow of electrons from the negative electrode to the positive electrode, through an external circuit, seeking equilibrium in the chemical potentials of both. In this process, the ions present in the negative electrode migrate through the electrolyte and insert themselves in the positive electrode (illustrated in Figure 2.1). This setup leads to the possible reversibility of the reactions, reversing this very process when during charging, as the ions can move from one electrode to the other through the cycles. The electrolyte is usually a liquid or gel that connects both electrodes, thus it must have low electron conductivity to prevent short-circuits, and serves as the conduit to allow ions to move between the electrodes in the cycling process. Besides these components, these batteries also include current collectors, to form a connection between the electrodes and the external circuit, and a separator, to further safeguard the separation between the electrodes and avoid short circuits. [9]

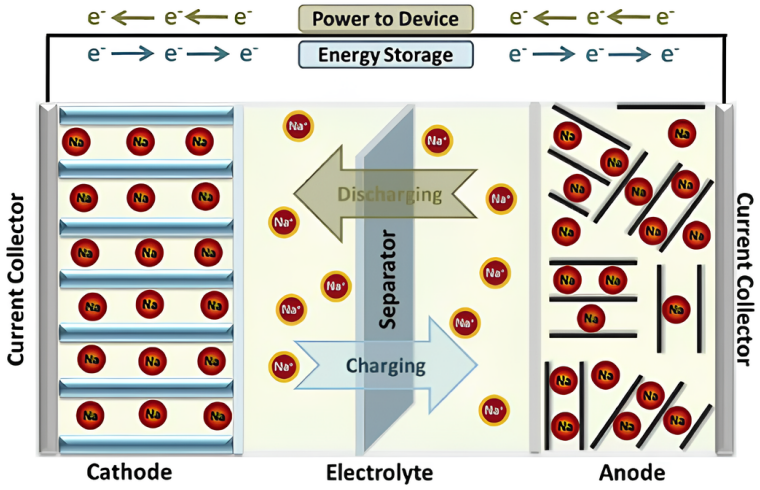

Figure 2.1: From [10]: Illustration of the composition and working of a sodium-ion battery

The most common and researched type of ion battery is the lithium-ion battery (LIB). Lithium is the third element of the periodic table and possesses a very low standard reduction potential, leading to batteries that can store more energy per volume unit. It presents a relatively small atomic radius, and subsequently a small ionic radius, an important element when dealing with the insertion and removal of these ions in the solid materials composing the electrodes, as it ensures a softer structural accommodation. Although LIBs are the most sought after, they are accompanied by a major challenge in their main component, as lithium raises concerns over long-term resource availability, costs, and the ability of supply chains keeping pace with rapidly growing global demand [11]. This has led to the search for other, more sustainable battery solutions that could rival LIBs, at least in some metrics and uses.

Sodium-ion batteries have been reported since the 80's, where a cell with hard carbon (HC) anode and polyethylene oxide cathode was assembled, in an attempt to create batteries analogous to their lithium counterparts [12], and studies on this technology continue well into the 90's [13]. At this time, LIBs were still under study, but as they evolved at a much faster pace and were much more promising in overall performance, researchers diverted focus on lithium cells and their materials. More interest started shifting towards SIBs once again with the search for more sustainable materials to possibly replace lithium. A neighbour to lithium in the Periodic table, sodium shares some characteristics with it, such as an electrochemical potential only 330 mV above lithium's and the same ionic behaviour, both tending to release an electron and become monovalent cations [14]. Thus,

these types of batteries function in remarkably similar ways, helping both the research and manufacturing transitions between the two, with sodium offering key differences in affordability and availability. Sodium is much more common in the Earth's crust, and it has the advantage of being less reactive, allowing for the use of some cheaper materials such as aluminium and iron in the internal battery components and reducing some safety concerns based on lithium reactivity.

Electrode materials and their crystal structures are often similar between the two technologies, and decide key characteristics in these batteries. Each electrode has a specific capacity, dictating the amount of electric charge they can hold per mass unit, and their composition offer different redox activation potentials, establishing the working voltage window for the full cell. In cathodes, compounds with transition metals that provide oxidation and reduction reactions are the most promising as they enable the insertion and removal of the ions. To fully accommodate the ions without compromising stability, the cathode's structure is of great importance, with both LIBs and SIBs having types of structures in common for these components, namely layered oxides and prussian blue analogues. The former is composed of several layers of a rock salt structure, wherein the ions intercalate in the vacancies formed in octahedral spaces between these layers, and has a composition generally defined as AMO_2, where A represents the alkali metal that will supply the ions, M is the chosen transition metal and O is oxygen. Given their 2D layered structure, some stability issues are present when the lattice tries to accommodate the ions, as it may result in permanent changes to the alignment of the layers. These issues are more prevalent in sodium, given its bigger size, and as a result layered oxides for SIBs have some different compositions when compared to LIBs, opting for iron and manganese based cathodes over the more common cobalt in lithium cells [11]. prussian blue analogue (PBA) are 3D cubic or rhombohedral structures with vacancies within their lattices, and as the ions are inserted their balanced structure can better accommodate and adapt to reach a stable phase. They have a general composition defined as $AM1[M2(CN)_6]H_2O$, where A represents the alkali metal, M1 and M2 represent two transition metals, C is carbon, N is nitrogen and H_2O is interstitial water. These cathodes are quite promising for SIBs as their adaptive structures are ideal for bigger ions, as depending on their composition they may shift from cubic to tetragonal or rhombohedral during the charge/discharge cycle. In the case of SIBs, they are once again mainly composed of iron and/or manganese [15]. Another cathode type, sharing the advantages of PBA's 3D structure, are polyanionic compounds, defined by the composition AM(XO4),

where A is the alkali metal, M a transition metal and XO4 a polyatomic anion, usually with phosphorus or sulfur accompanying the oxygen. These structures are often highly stable, allow good reversible ion insertion/removal and offer high potentials, yet often offer lower capacity and conductivity than their counter parts [16].

As for the anodes, the most common materials are carbon based compounds. Metallic alloys of the main ionic component are options that promise higher specific capacity, but are generally overlooked as they present severe volume change issues and, in the case of SIBs, safety concerns over the development of dendrites. For LIBs, the main carbon compound used is graphite, as it offers great electronic conductivity, stable structure and a general low cost. This has seen widespread use as the most common LIB anode, and so naturally it has been tested in SIBs, but with little to no success. The bigger ionic radius cannot insert properly in the graphite structure, leading to extremely low capacity in sodium-ion cells. As an alternative, hard carbon anodes have proven to be much more apt for SIBs, with a larger interlayer spacing ideal to accommodate sodium ions [17]. These anodes also exhibit great solid electrolyte interface formation, a solid interfacial layer formed with the first few charge/discharge cycles, between the anode and the electrolyte, that, when well formed, provides protection for both these components, prevents electron flow through the electrolyte and improves the stability of the battery. It is formed through side reactions that consume ions and result in losing some working capacity [18]. Currently, SIBs present a lower energy density than LIBs, but due to their low material cost they have a better cost per kilowatt-hour (kWh), suitable for stationary energy storage cases where size and weight are much less restrained (such as electrical grid uses) [19]. The biggest concern about SIBs compared to LIBs are related to the bigger atomic and ionic radius in sodium (1.02Å as opposed to 0.76 Å for lithium [10]), this leads to the lower energy density and aggravates the cell's structural degradation, as a result of the recurring intercalation and removal of ions in the electrodes.

2.2. Ageing in Ion Batteries

Battery degradation or aging is a very important subject when discussing these technologies, as a device that cannot last for extended periods of time, or that cannot be used extensively, is of no general use, especially when considering sustainability concerns. Studies on batteries' general aging and state of health (SoH), with focus to understanding degradation and its specific mechanisms, have become increasingly more popular in

recent years as new battery applications like electric vehicles and electrical grids have gathered more attention [20].

There are two types of aging, calendar aging and cyclic aging. The former refers to the degradation occurring within stored batteries that do not forego any electrical use and thus degrade on their own through time. As for cyclic aging, the focus of this work, refers to the degradation incited by the active use in charge and discharge cycles of the device. This type of aging leaves more room for experimentation and variability, as any change in the cycling profile may or may not affect the final degradation.

Many studies have been led trying to find ways to extend the overall life cycle of energy storage devices, be it through new electrode or electrolyte materials, different storage or working conditions. With time, degradation on a cell is identified with the loss of energy storage capacity (*C* or *Q*) and the rise of internal resistances [21]. The first is a metric that can be calculated through integrating the electrical current (*i(t)*) running through the battery over a certain period of time (*T*), usually a full charge or discharge 2.1. The number of cycles a battery may maintain a good useful capacity for is very dependent on the battery itself, the components and manufacturer. Many studies rely on a state of health metric, based on the percentage of current available/working capacity in relation to the total, initial capacity.

$$C = \frac{1}{3600} \int_T i(t)dt \tag{2.1}$$

Another metric used is the coulombic efficiency (CE), an efficiency calculated for a single full cycle comparing the cell's capacity when charging and when discharging2.2. An ideal battery should keep the same capacity in both steps, and most of the time the efficiency should be in the high 90% in a decent battery, but with certain degradation mechanisms this balance may be affected, having either the charge or discharge steps hold more capacity than the other. Sudden changes in this efficiency might signify side reactions, loss of ion inventory, ion trapping, or significant damage to one of the electrodes. [22]

$$CE(\%) = \frac{C_{discharge}}{C_{charge}} * 100 \tag{2.2}$$

The differential capacity (or incremental capacity) curve is a metric calculated through the derivative of the capacity in regard to the battery's voltage, as dQ/dV. This curve

is represented in a single, whole charge/discharge cycle, as a function of voltage, and presents several peaks, where each of them correspond to the main redox reactions or phase transitions happening within the battery. Comparing these curves in several cycles, as these peaks wane, change intensity, location and overall shape, they signal specific degradation mechanisms taking place internally through the cycling process [23]. As they correspond to these phase shifts and redox reactions, this curve is useful to evaluate the degradation on the electrodes, both positive and negative, showing their overall change in performance with aging.

Several other metrics change with the cell's aging, such as the time it takes to reach the voltage limits (Voltage vs. Time), as a shorter time to reach higher potentials under the same current may indicate severe resistance raise, and changes in the curve's shape indicate a shift in the inner reactions of the battery.

Analysing the electrical current in both charge and discharge over time (Current vs. Time) provides a way to properly evaluate, through the cycles, if the designated cycling profile is being fully accomplished, as some degradation or damage may lead to certain steps being shortened or even skipped.

As for resistances, the internal impedance of a battery can be determined with a widely used test called electrochemical impedance spectroscopy (EIS), and plotting these impedances and resistances can highlight the specific components in the cells that suffered the most damage and explain the changes in the battery's behaviour observed in other curves.

These metrics, tests and techniques help build the full image of the electrochemical, kinetic and physical phenomena that occur with the recuring cyclic aging, leading studies on their degradation mechanisms. Understanding these mechanisms is the key to better understand the inner workings of this technology and further optimize the full lifetime [24].

2.3. Degradation Mechanisms

As for the specific mechanisms that may occur within the battery, it is important to understand in what ways can each component of the cell contribute to the overall aging. The increase in internal impedance and resistance may be a result of side reactions altering the path of the electrons and ions within the structure. Some of these reactions are beneficial to the inner workings of the battery, such as the solid electrolyte interface, which, when correctly formed, provides fast transport for the ions and is a good electronic insulator to prevent further electrolyte degradation [25]. But, when the SEI is malformed,

uneven or too thick, this may lead to a detrimental impact on the stability of the system, as it might result in the partial dissolution of the layer causing self-discharge and eventual damage to the battery. The malformation may also be a sign of trapped solvated ions, which may form metallic clusters that greatly impede the ion mobility and increase the overall charge transfer resistance [26]. There are further reports of metallic plating forming within the structure, with the process illustrated in Figure 2.2, usually when cycling at lower temperatures, resulting in loss of ion inventory, decreased capacity and higher resistance [27].

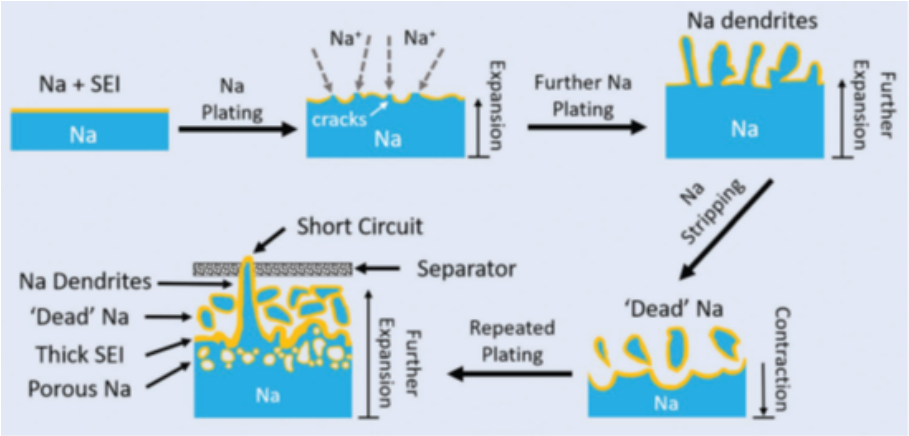

Figure 2.2: From [28]: Illustration of SEI growth and general decrease of capacity in a SIB

In the electrodes, the continuous insertion and removal of ions within its solid structure, especially in the case for SIBs with the bigger ionic radius for sodium, causes severe volume change, such is the case reported in [29], presenting 22% volume change in the cathode, leading to instability in the crystal lattice. This may in turn lead to loss of electrochemically active material, structural cracking, resulting in poor electrical contact with the rest of the cell, causing difficulty in the ionic insertion/removal and in their respective mobility between components, driving up the internal impedance [30].

The structure of the electrodes influences which mechanisms are more common, thus it is important to consider the materials at work in degradation studies. With the use of transition metals in the cathodes, the Jahn-Teller (JT) effect is considerably common. It is a phenomenon that takes place in non-linear molecular systems in electronic degeneracy, meaning there is an uneven distribution of electrons within the orbitals. Seeking balance by removing these degeneracies, there is a subsequent loss of symmetry, structural distortion and decrease of total energy, affecting the inner working of the battery

and degrading its performance [31]. In layered oxides, surface decomposition is commonly observed, as parasitic reactions with the electrolyte often result in dissolution and deposition of the transition metals in their interface which cause loss of capacity. Internal cracking and random surface crystal reconstruction may also occur, leading to impedance and resistance raise [32]. As for PBAs, surface degradation leads to the interstitial water seeping into the electrolyte, greatly affecting ionic conductivity, and, in cases of organic carbonate electrolytes, reactions may result in CO2 and gassing issues within the cell, causing volume expansion and potential safety risks. These cathodes also exhibit collapse of their crystal structure under cyclic aging, resulting in transition metal dissolution [33]. Structural damage might also result in full phase transitions in the electrodes, and as their composition changes it results in less pronounced redox reactions in the active materials, causing a lower total capacity of the cell [34]. For cathodes like PBAs, where the insertion and removal mechanisms are accompanied by reversible phase transitions, the structural stress and volume change they provide may cause certain transitions to be irreversible, leading to a collapse of the cell's inner chemistry.

In the anodes, most degradation is related to the formation of the SEI layer, as if it is malformed it may damage the electrode surface, damaging the lattice structure. In the case of hard carbon, the vacancies in it's crystal structure may lead to ion trapping, decreasing the overall working capacity of the battery and, once releasing these trapped ions, the excessive thickening of the SEI [35].

2.4. Testing Protocols in the Literature

To fully grasp which of these mechanisms occur in each device, several electrochemical tests and characterization techniques are usually put to use in their research. They may vary from standard tests while cycling (in operando), to evaluate the SoH or the working capacity of the cell at that moment, to after the battery is considered "dead" and won't have any further use (post mortem), to evaluate the full destruction and aging that took place. The latter also has a distinction between tests that cause irreparable damage to the cell, that are invasive and require physically opening it, referred as destructive procedures [36].

Among the first kind are the curves obtained from the standard units and measurements taken while cycling, although the available data may depend on what equipment is being used. The simplest of metrics is the evolution of capacity in each cycle. This may give great inner detail about what happened inside the cell and at around which cycle, which

is a great metric to have as auxiliary to the others. Any sudden tendencies of huge drops, spikes or several cycles stable at a certain value all indicate severe change or damage in the battery's chemistry and composition [37]. Although useful, it is a limited representation of degradation, as it can't fully demonstrate which specific mechanism or damage have taken place. For a more specific analysis, other curves are observed, such as the aforementioned voltage and current through time curves.

As for postmortem tests, a widely utilized measure is the previously mentioned EIS. It is based on how an electrochemical system, when subjected to an input signal, will produce an output signal. Thus, by feeding our system (a battery in this case) certain sinusoidal signals, with either alternating current (galvanostatic) or alternating voltage (potentiostatic), and ranging in the signals' frequency from higher values ($10^4 Hz$) to lower ($10^{-2} Hz$), several responsive output signals can be read. Be it, for example, that the input potentiostatic signal is known, measuring the output alternating current signal allows the internal impedance to be extracted by relating both signals [38].

$$Z(\omega) = Z^{'} + jZ^{'} \tag{2.3}$$

The resulting values for impedance (Z) are represented as complex numbers, with a real and an imaginary component. These components are represented in a curve with the imaginary part in the vertical axis and the real part in the horizontal one, this is called a Nyquist plot. These graphics present expected tendencies, usually either straight lines or semi circles, and they may represent resistive or reactive components (or both). Analysing the whole curve and the respective components leads to the development of an equivalent circuit, as in a circuit that would simulate the impedance of the battery as closely as possible. These circuits are composed of resistive elements (R), capacitive elements (C) and constant phase element (CPE). While these elements do not directly correlate to a specific physical component in the device, they are meant to represent certain behaviours, thus monitoring their evolution within an aged cell can provide useful insight into the internal degradation [39]. Figure 3 illustrates a Nyquist plot similar to what would be expected of a battery, and the respective equivalent circuit above it.

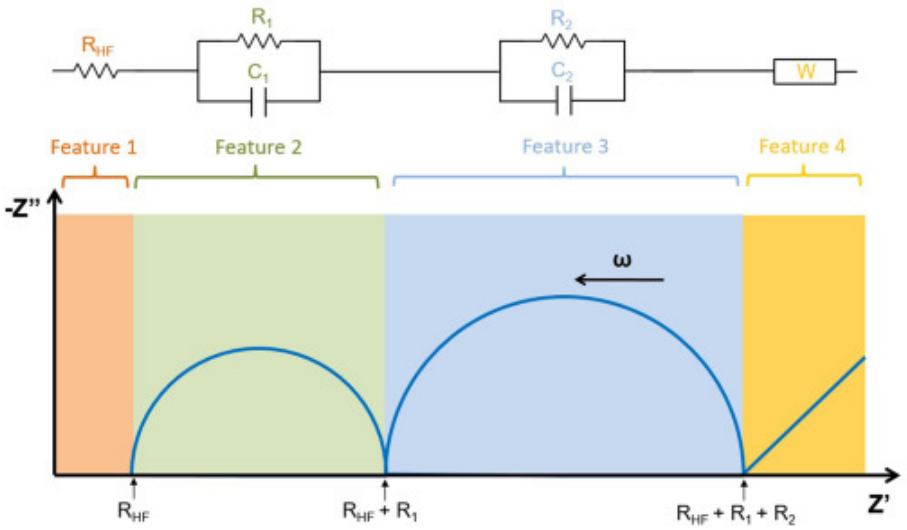

Figure 2.3: From [39]: Schematic of EIS nyquist plot of a multicomponent system with a respective equivalent circuit above

When comparing the initial Nyquist curve with subsequent ones, be it impedance values taken at certain intervals of cycles or just the final postmortem EIS, further knowledge is gained of the inner shifts and changes in the device. Each section of a Nyquist plot corresponds to different sectors within the battery, starting, from highest to lowest frequency, with the Electrolyte impedance (usually a small straight line, bellow 0 for the imaginary impedance), the SEI and general interface impedance (a semi-circle, includes most of the points in the curve) and the impedance within the electrodes (a rising slope, referred as a Warburg tail, correspondent to ion diffusion). [40]

Considering the supposed Nyquist curve of a battery, and the initial curve of the cell at hand, analysing from where the raise or shift in impedance has originated is a case of comparing the differences between the non-degraded and the degraded EIS. As an example, in the study presented in [41], the impedances of two batteries were compared, one with an aged electrode and another with an intact electrode. The aged electrode is clearly recognisable by the much larger impedance values and the overexaggerated semicircle.

Destructive measures, as the name indicates, destroy the batteries' structure and make it ultimately unusable, in order to better analyse the inner components. As these cells tend to be composed of volatile and reactive materials, especially with certain elements present in the atmosphere like oxygen, these destructive tests are performed in glove boxes, under controlled, inert atmospheres composed usually of argon or other inert gases. Given the nature of these techniques, to have any reference point of an uncycled battery to compare

to the final results, a different cell from the same manufacturer must be used. scanning electron microscopy (SEM) is a technique that uses a focused beam of electrodes to scan a materials surface, and may be used to observe the topology and constitution of the electrode materials, evidencing certain changes, cracks or even dissolutions of certain materials [42]. Another usual technique used is X-ray diffraction (XRD), consisting of bouncing X.rays onto a material sample and registering the diffracted (or scattered) rays. It presents very specific peak patterns for the respective elements present in the studied sample, so it has an added use as a characterisation technique to discover or confirm the composition of the electrodes. As the peaks represent specific patterns, this can be used to confirm any alterations in the structure or composition of the battery component under study, by observing the differences between a cycled and an uncycled cell [43].

2.5. Protocols and Expected results

In many instances, batteries won't be used with perfectly controlled cycling conditions. Variables such as temperature, surge currents, early/late stopping conditions to charging or discharging, many uses of energy storage have less then constant conditions, and because of this, it is important to properly study how a device reacts under different situations. When applied to the study of cyclic aging of batteries, this is evaluated by applying varying charging and discharging protocols, and repeating them for several cycles to observe the degradation mechanisms that take place in their specific conditions.

One simple change that can be done to the charge/discharge protocols is changing the working electrical current. Usually measured in C-rates, a measurement of current relative to the working battery's full capacity, where a 1C C-rate signifies the electrical current needed to fully charge or discharge the cell in 1 hour time. There are the simpler protocols which simply change the values as constant current (CC) for both charge and discharge at the same value, and others that aim for different values at each step [44]. These studies aim to find a correlation between the cycling current and the degradation, where theoretically the battery aging should accelerate with the more aggressive, higher currents. This may be explained with general malformation of the SEI layer and further cracking of it and other components such as the electrodes. This is even boosted by the higher internal temperatures from cycling at higher currents, leading into possible formation of compressed gases within the cell than end up pressuring and damaging the components. This in turn leads to a bigger loss of both primary (ion inventory) and secondary (electrode) materials,

and a higher internal impedance, causing more deterioration in the cell [45]. Another factor that attracts many studies is the state of charge of the battery. The SoC describes the current state of the battery in terms of remaining capacity, indicating a fully charged cell as having 100% SoC. In many cases these metrics are controlled by limiting the working voltage in the cycles, and have the adverse effect of limiting the total working capacity of the cell. These protocols enable the specific study of degradation mechanisms that take place or are promoted by either high or low potential and SoC, as well as the effects of not using the device's full available capacity. As a result, studies have looked into the possible optimization of SoC use, by evaluating the degradation tendencies of very specific SoC values, such as in [46] using intervals of 10% of SoC, although the study ends up overlooking the specific mechanisms that take place. Other studies focus on the use of a bigger portion of the battery's capacity by using wider ranges of SoC, thus observing and fully studying the degradation mechanisms present within those ranges in scenarios where a bigger, more extensive cycle occurs. In [47], several intervals were tested with multiple batteries, and it was discovered that the more extreme ones (on the lower/higher ends of the SoC percentage) were significantly more degraded than their more central counterparts. This might be explained by how in the more extreme values of SoC there is an uneven distribution of the total ion inventory, which might cause some strain on the electrodes.

An interesting perspective to analyse in the cycling conditions is the overall signal shape, usually used as a simple constant current signal, but in many real world instances the current flowing through the battery won't be so constant. This leads to studies observing degradation in protocols like a stepped charge/discharge [48], where several timed CC steps are sequenced in a descending or ascending order of current rate. Another highly studied signal shape is the pulsed charge or discharge, where the signal rapidly varies between two "modes" in a wave like periodic manner. These varying "modes" can realistically be anything, with the most common types of pulses being the pulse charge rest (PCR), where each period of the signal correspond to a CC charge and a rest time, a pulse charge charge (PCC), where the rest step is traded for another CC charge with a different value, and pulse charge discharge (PCD), where the variation is between a higher current CC charge and a lower current CC discharge (illustrated in Figure 4) [49]. It is suggested that these types of protocols can shorten the overall charging time, by lowering the total ion concentration in charge transfer, and reduce risk of overheating the

battery, as they are less straining than the constant electrical current powering the standard CC cycles. It is also found that it reduces the internal polarization voltage with a smoother intercalation of the ions into the electrodes, which in turn leads to less strain on these components [50]. With the more complex signal shape come more variables to set, such as the active frequency, the pulse duty cycle and amplitude, and when not finely tuned these might lead to promoting certain habits of overcharging and overvoltage in the battery, hurting the overall performance and durability [51].

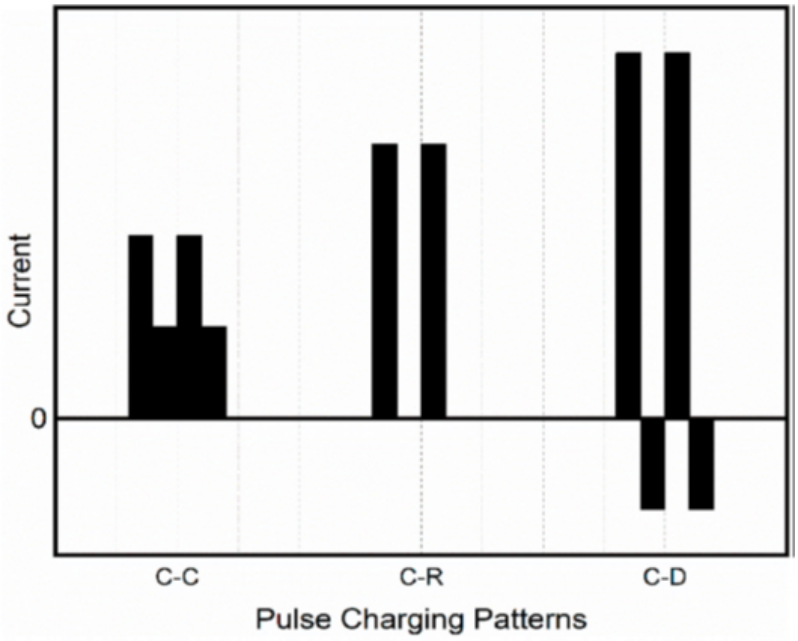

Figure 2.4: From [49]: Examples of the pulse charging profiles described above

These protocols are meant to test for ways to protect the battery and extend the cycle life, but there are also destructive protocols meant to push the limits on the cell's degradation. One example of these destructive profiles is the overcharge, where the battery is charged way above the supposed safety voltage limit, further observing the mechanisms that activate at high potentials. This is very important for safety concerns, to understand how the battery would react to unforeseen or unexpected conditions in the real world. These protocols usually lead to a higher working capacity in the first few cycles, which quickly fades into full degradation with very few cycles. In fact, the higher the overcharge potential the quicker the capacity fades, as the cathode is usually stripped of all ions and active materials (other lithium or sodium atoms present in the electrode) beyond the reversible limit. This causes electrolyte degradation and, on the anode side, some plating as the anode reaches its insertion limits, thus forcing extra ions to accumulate and plate. These

mechanisms increase the internal resistances and, in turn, the internal temperature of the cell when cycling [52].

Another destructive protocol is in increasing the current C-rate beyond the safety limits. In this case, the ultra-high current should lead to a faster aging, as new degradation mechanisms are provoked by the faster cycles. LAM suddenly becomes much more significant in the battery's degradation, as the steep C-rates lead to excessive and aggressive charge/discharge. In turn, this lowers the total capacity of the electrodes and leads to internal plating, translating into raising resistance and impedance in the cell [53].

2.6. Current State of SIB Cyclic Aging Studies

As previously stated, the possibilities and potential of SIBs have been documented for a few decades, but intensive study on this technology only gathered more attention in recent years. Even further, as these batteries often have lower benchmark metrics when compared to LIBs, most studies have focused on finding better and more efficient materials and components to improve their performance. This lead to a lack of articles on general SIB aging and degradation mechanisms, when compared to its lithium counterparts, and even the few degradation studies available are often performed on half-cells, being much harder to find cases of full-cell studies. One such case is the study [54], conducted in 2022, reported as the first of its kind, that analyses both the calendar and cyclic aging of commercial 18650-format SIB full cells, focusing on the observed degradation mechanisms. They have a hard carbon (HC) anode with a polyanionic $Na_3V_2(PO_4)_2F_3$ (NVPF) cathode, manufactured as part of the authors work, building 36 units at their disposal. On the calendar aging side, 12 cells were used, kept at different temperatures (5ºC, 25ºC or 45ºC) and at different states of charge (30%, 50% or 100%), and as for the batteries under cyclic aging, 12 were used and distributed in a protocol matrix varying the working temperature (25ºC or 45ºC) and the charge/discharge C-rate (0.2C, 1C or 2C). For each test, two cells were used to ensure reproducibility and trust in the acquired data. To evaluate the performance of the devices, check-up tests were periodically employed, more complete in the first and last instances to further characterize the behaviour of the cells, measuring energy and capacity retention with varying C-rate and discharge resistance at several SoC and temperatures. At the end of life, the batteries were dismantled, and their components were subjected to several characterization techniques, such as XRD and Na-solid state nuclear magnetic resonance (NMR) and P-solid state nuclear magnetic resonance (PMR).

For the calendar aged cells, they were separated in two groups: 6 cells stored at 100% SoC at different temperatures and 6 cells stored at 25ºC at different SoC levels, in order to properly test the effect of both metrics individually, and both were stored for around a year. In both cases, the analysed metrics were the capacity loss and internal resistance throughout the storage time, and the end of life discharge capacity. In regard to the temperature, it seems to affect the aging due to a relatively lower electrolyte stability with higher temperature, and as for the SoC, at 100% the resistance increases due to higher electrolyte degradation and contact with fully charged electrodes. A similar analysis was applied to the cyclic aged cells, but instead of the storage time the capacity loss curve was used in regard to the number of cycles. Once again, higher temperatures yielded more capacity loss, and lower C-rates seemed to show the same trend, suspected as an effect of faster electrolyte degradation promoted by more time spent at higher SoC values. These results are further corroborated and interpreted with the help of the post-mortem characterizations. XRD detected some structural modifications, as the positive electrode showed multiple phases different from the initial material and general inhomogeneity, most likely caused by the internal temperature gradient formed on the cycled batteries. The change in composition and phase are more likely due to a general loss of Na ion inventory, most of it in the first few cycles due to SEI formation.

In the end, the study provided proof of how the storage and cycling conditions affected the aging of the cells, and how the degradation mechanisms could be identified, providing a good framework of how these degradation studies can be conducted. This was further developed in future studies that tackled similar issues, such as [55]. This article presents a bigger focus on the initial battery categorization, but tests the cyclic and calendar aging of some cells, finding once again the SEI formation to be a common source of capacity fade in SIBs. It also demonstrates the expected evolution of the EIS curve in cyclic aged batteries, how the ohmic resistance increases over the cycles and a second semi-circle appears, with general change in the charge transfer and diffusion regions of the graph indicating change in the electrolyte ion transfer and possible damage to either the electrodes or their interfaces. Most studies determine these interfaces as a large cause of impedance raise and ion inventory consumption, be it through SEI formation or even lithium plating in other cases [56]. This plating eventually leads to more sodium reactions within the electrolyte, compromising the standard functioning of the cell and causing a possible safety hazard.

As for possible damage in the electrodes, it may be related to cracking, which also has

consequences on the electrode-electrolyte interface, thus raising internal impedance, as this is reported in many cathode materials [57]. This seems to be more common in SIBs over their lithium counterparts in large part due to the bigger atom/ion radius, as their insertion and removal cause much more structural damage, also leading to possible dissolution of active material. This difference in size also affects the ion diffusion within the electrodes, usually in the HC anodes, causing the cathode to experience high local potentials due to diffusional polarization and leading to loss of active material. In the degradation study [58], upon closer inspection of the cycled cells, in a polyanionic cathode, several microscopic sodium-oxygen spheres were forming, causing the general loss of sodium inventory and capacity as well. Taking into account literature for LIBs, along with the limited literature for SIBs, the most common and dominant degradation mechanism should be general loss of ion inventory, mostly due to side reactions like SEI formation and metal plating. This is mostly applied to standard cycling protocols, as for protocols that are more aggressive on the electrodes may lead to LAM and electrode cracking and volume gain to become more dominant in the overall aging. General studies of the effects of different cycling conditions (other than C-rate and temperature) are lacking in the current research landscape, therefore our current understanding of their degradation under more realistic uses is still relatively small. Thus, it is critical to better study and analyse these mechanisms and how different they are under different conditions, to guarantee that SIBs are real alternative to LIBs in real, practical uses.

3. Experimental Methods

3.1. Materials and Equipment

A total of 29 commercial grade 18650 cylindrical format sodium-ion cells manufactured by Shenzhen Zhonghuajia Tecnology Co, Ltd were provided for this study. The composition of their components is unknown. Its nominal capacity is 1.5 Ah, with a nominal voltage of 3.1 V. The potential working limits are defined between 1.5 V up to 4.1 V, the working temperature ranges are from -10ºC to 45ºC and -30ºC to 60ºC for charge and discharge, respectively. For the C-rate limits, at standard room temperature around 20ºC-25ºC, which is the temperature this study will be working under, the maximum current for a CC charge is 1C and for a CC discharge it's 3C. The batteries have a mass of 37 g, an internal resistance under 20 mΩ, and an energy density of 128 Wh/Kg.

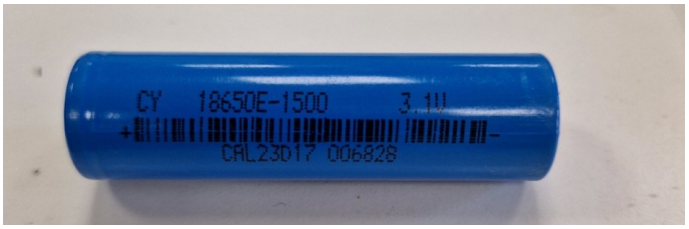

Figure 3.1: Photo of one of the cylindrical batteries used in this study

To perform the charge and discharge cycling, two Landt CT3002K battery tester units were used, each connected to their respective controlling computers and each with 8 channels. These channels were connected to plastic battery holders with gold connectors, most for 18650 format but some for 21700 format, all of which were assembled in the lab. The protocols were developed in the Landt battery tester software, named and identified, and the resulting data from the cycles was routinely extracted and exported in the form of CSV files with as much data about the process as possible. These were organized in columns with all the possible data the device would provide, but the most important measurements were the charge/discharge capacity, voltage, electrical current, coulombic efficiency, differential capacity and test time.

To further ensure completely equal starting conditions for all cells and provide a better, more fair comparison of their cycle lives in the future, before every protocol 2 standardized break-in cycles were performed. These cycles consist of a CC-CV charge, where a C-rate current of 0.5C is applied until the unit reaches the upper cutoff voltage and is then

followed by a CV step where it is maintained at that voltage until the provided current reaches the cutoff limit of 0.05C, or until the maximum safety capacity is reached. The same process is applied to the discharge, thus guaranteeing every battery begins their protocol from a fully discharged state.

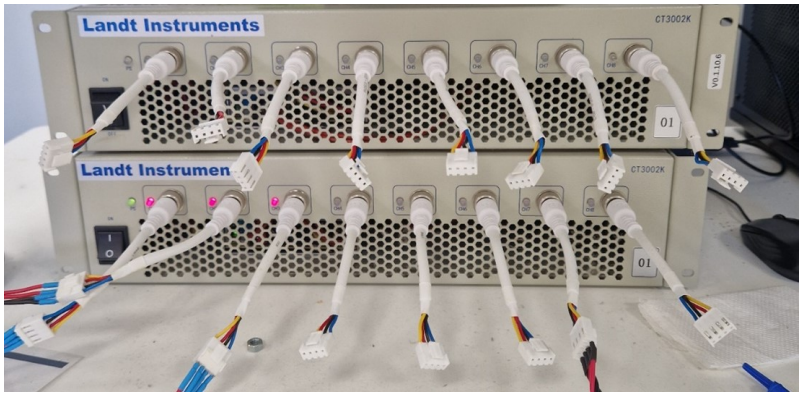

Figure 3.2: Two Landt CT3002K battery tester systems, stacked on top of eachother

For further characterization and insight into the battery degradation, we perform two EIS tests, one before and one after cycling, in order to compare both and analyse any source of impedance change. An Arbin Laboratory Battery Tester LBT21084, coupled with a Gammry Interface 1010E, were used to perform them, with the Arbin software used to export the data as CSV files. A battery was used to test the parameters for the EIS procedure to be set, as we tested multiple frequency ranges, voltage values (if potentiostatic) and current values (if galvanostatic). The better results were identified for a voltage range between 10 mHz up to 50 kHz, in galvanostatic mode, with an AC current of C/200 (about 7.5 mA) RMS.

All the extracted CSV files were analysed and handled with python, using the packages pandas and *impedeance*, and the curves and graphs represented with *matplotlib.pyplot*.

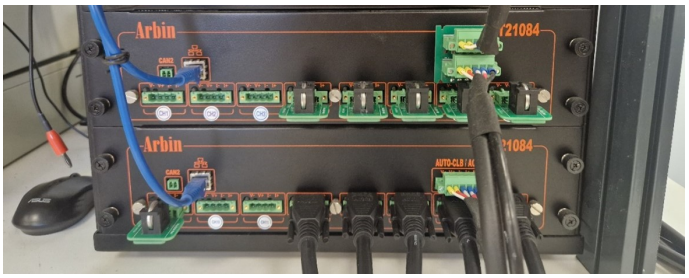

Figure 3.3: Arbin Laboratory Battery Tester LBT21084

Figure 3.4: Gamry Interface 1010E

3.2. Experimental Protocols

In a laboratory setting, the batteries were identified as BF-N, with N being the battery number in order they were used, but for better reading purposes they were renamed to codes relating to their specific cycling profiles in this work. Each protocol was tested with at least 2 cells, to ensure reproducibility, and some were applied on up to 4 cells. For better organization, all protocols were split into four groups, with respect to their similarities.

3.2.1 C-Rate Variation

The first group is identified by the code CR, for C-rate, and an accompanying number representing the C-rate current and maintaining within each profile an identifier -N for each different cell used (for example, 1CR-1 for a cell tested at 1C C-rate, CR/5-1 for a cell tested at 1/5 C-rate). These profiles consist of simple constant current charge and discharge at a set C-rate, within the full limits of voltage. As such, the effects of a faster or slower cycle is put to the test, as well as the consequences of having a faster, more aggressive charge removal/insertion in the electrodes. They were based on the protocols used in [54], with an added protocol at 3C to further test a more extreme case.

Table 3.1: Batteries tested under C-rate variation protocols

Protocol	Label	CC Charge	CV Charge	CC Discharge	CV discharge
Standard cycle at 0.2C	CR/5-1	0.2C	No	0.2C	No
	CR/5-2				
Standard cycle at 1C	1CR-1	1C		1C	
	1CR-2				
	1CR-3				
Standard cycle at 2C	2CR-1	2C		2C	
	2CR-2				
Standard cycle at 3C	3CR-1	3C		3C	
	3CR-2				

3.2.2 SoC Window Control

The second group consists of protocols testing the effects of the working SoC in the profile, consisting of profiles charged and discharged at a constant C-rate, but with varying voltage limits, to control the cell's SoC. The specific values are set by analysing the open circuit voltage (OCV) vs SoC curve provided in the battery datasheet, and for these cases the important values are: 0% → 1.5 V ; 20% → 2.6 V ; 80% → 3.8 V ; 100% → 4.1 V. These profiles were loosely based on the cyclic conditions of both [59] and [60], but slightly tweaked to better accommodate time constraints and our number of available batteries. Thus, 3 different ranges were defined, one to test the effects of high SoC (20% - 100%, SCup), one to test low SoC (0% - 80%, SCdown) and one that avoided both (20% - 80%, SClim). This way it can be identifiable the effects of the higher and lower SoC values, as well as testing a more conservative and protective protocol that avoids both. As a standard cycle reference, the protocol 1CR was used, this way a fair comparison could be drawn by keeping these protocols cycling at 1C current C-rate.

Table 3.2: Batteries tested under SoC window variation protocols

Protocol	Label	CC Charge	CC Discharge	Voltage Range	SoC Variation (%)
Standard cycle at 1C	1CR-1	1C	1C	1.5V - 4.1V	100%
	1CR-2				
	1CR-3				
Limited SoC 20%-80%	SClim-1			2.6V - 3.8V	60%
	SClim-2				
Limited SoC 20%-100%	SCup-1			2.6V - 4.1V	80%
	SCup-2				
Limited SoC 0%-80%	SCdown-1			1.5V - 3.8V	80%
	SCdown-2				

3.2.3 Pulse Profiles

The third group consists of batteries cycled under pulse profiles. Largely based on the profiles exemplified in [49] for pulse charge-rest (PCR) and pulse charge-charge (PCC). Pulse charge-discharge was attempted, but unfortunately due to the way the Landt battery tester counts cycles the data was impossible to properly comprehend and analyse, thus this protocol was dropped. As for the other two, once again to use 1CR as a standard cycle reference, both were kept with an average current of 1C C-rate, meaning the pulse charge-rest had a charge stage of 2C to average the rest stage of 0C, and the pulse charge-charge had alternating currents between 1.5C and 0.5C. In both cases the total

duration of one pulse is a minute, equally divided by the two steps it consists of. These are more conservative protocols and are meant to test if changing from the typical constant current cycle will provide significant change in aging.

Table 3.3: Batteries tested under different pulse profile protocols

Protocol	Label	CC Charge	CC Discharge	Pulse Duration
Standard cycle at 1C	1CR-1	1C	1C	Constant
	1CR-2			
	1CR-3			
Pulse Charge-Rest	PCR-1	2C/0C	2C/0C	1min. / 1min.
	PCR-2			
Pulse Charge-Charge	PCC-1	1.5C/0.5C	1.5C/0.5C	
	PCC-2			

3.2.4 CC-CV and Asymmetrical profiles

The final group is slightly more miscellaneous, as the common element is the use of a constant voltage (CV) step after charging, and in some cases after discharging as well. The simpler ones consist of simple CC-CV charge/discharge cycles, one at 0.5C and the other at 1C, largely based on the cycles used in [61], to better understand the effects of fully charging and discharging the battery, and if this extra step would contribute to any degradation mechanism in any way. The others only have the CV step present in charging, mimicking the standard protocol set in the data sheet, performed in this batch, and adapted to a fast charge, a fast discharge and a stepped discharge protocol. These last three weren't as much based on available literature, but more so on imitating some more real life uses, such as fast charging a device, a device that requires intensive discharge or a more every day device being used in certain intervals, instead of being discharged constantly. As such these cases will give insight into how the batteries may age under non ideal conditions.

Table 3.4: Batteries tested under different CC-CV and asymmetrical protocols

Protocol	Label	CC Charge	CV Charge	CC Discharge	CV discharge
Standard cycle at 1C	1CR-1	1C	No	1C	No
	1CR-2				
	1CR-3				
Full cycle at 1C	FC1C-1		Yes - cutoff at 0.05C		Yes - cutoff at 0.05C
	FC1C-2				
Full cycle at 0.5C	FCC/2-1	0.5C		0.5C	
	FCC/2-2				
Datasheet protocol	DS-1			1C	No
	DS-2				
Fast discharge	FastDC-1			3C	
	FastDC-2				
Stepped discharge	StepDC-1			1C steps of 0.4V	
	StepDC-2				

4. Results and Discussion

4.1. Battery Materials Characterization

To better understand the effects the aging protocols will have on the batteries, an initial characterization of our cells was developed. This consists mostly of the EIS Nyquist plots before they were cycled and its respective equivalent circuit, along with an analysis of the differential capacity curve of the batteries to compare to literature and discover the electrode materials we will be working with.

As for the internal impedances, there is a common equivalent circuit used to describe energy storage devices, the Randles circuits. It consists of a real resistance, R0, in series with the parallel combination of a double layer capacitor, C1, with a resistor and a faradaic impedance element (Zw), R1 and W1, respectively. To ensure a good fit on our results was obtained, 3 other variations of this circuit were tested. One variation was an alternate Randles circuit, but instead of a simple capacitor it had a constant phase element (CPE). The other two were variations of these Randles circuits, but with the faradaic impedance element outside of the parallel circuit. They are illustrated in figure 4.1.

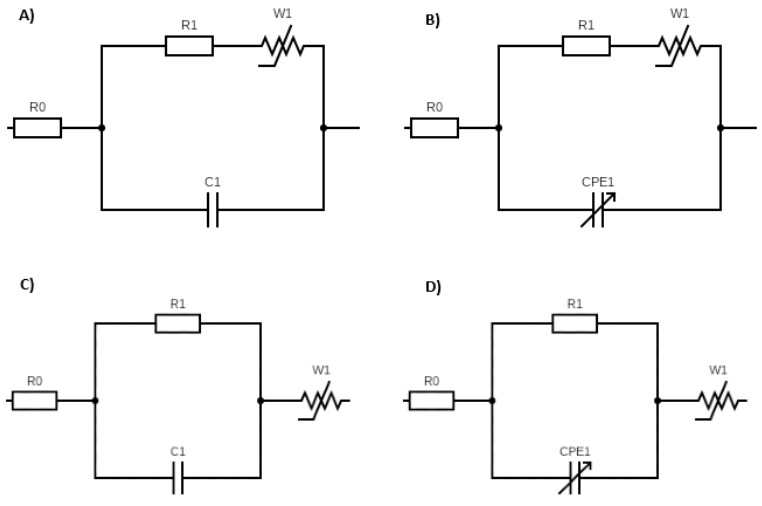

Figure 4.1: Equivalent circuits used for EIS fitting, with Randles circuit (A), alternate Randles circuit (B), custom circuit (C) and alternate custom circuit (C)

Out of all the circuits fitted, the initial Nyquist curves of the uncycled batteries better corresponded to the behaviour of the alternate custom circuit (D in figure 4.1). In this circuit,

we have an initial resistance, R0, representing interfacial layer such as the SEI, a semi-circle dictated by the parallel resistor R1 and the constant phase element CPE1, as the impedance for internal ion movement and conductivity, and at the end a defined Warburg tail, corresponding to ion diffusion within the electrodes, with a faradaic impedance element W1. The purpose of separating W1 from the parallel portion of the circuit is to have the ion conductivity semicircle and the Warburg tail portions of the Nyquist plots be more independent in order to better fit the data. It should be noted that the data used for these fits did not include the batteries 1CR-1, 1CR-4, FCC/2-1, FCC/2-2, FastC-1, FastDC-1 and FastDC-2, as these batteries were cycled before the final EIS protocol was defined.

Using the *python* package *impedance*, we can plot our data, develop our determined circuits, make an initial guess for their elements, fit them to our data and determine the values of the fitted circuit. This initial guess was loosely based on the observable values observed at a Nyquist plot for the batteries. After obtaining the EIS data for all uncycled batteries, the values of each element of the fitted circuit were saved to a file, and then the mean value for each of them was calculated, obtaining the following table:

Elements	Values	Values
R0	$(2.26 \pm 0.15) \times 10^{-2}\ \Omega$	-
R1	$(1.07 \pm 0.07) \times 10^{-1}\ \Omega$	-
CPE1	$(3.86 \pm 0.13) \times 10^{-1}\ \Omega^{-1} s^{a}$	$(7.74 \pm 0.05) \times 10^{-1}$
W1	$(7.95 \pm 0.88) \times 10^{-2}\ \Omega$	$(217.63 \pm 15.66) s$

Table 4.1: Average values of each of the equivalent circuit's elements

Applying these mean values to the circuit, and forming a prediction with our range of frequencies used, the average Nyquist curve of these batteries can be traced:

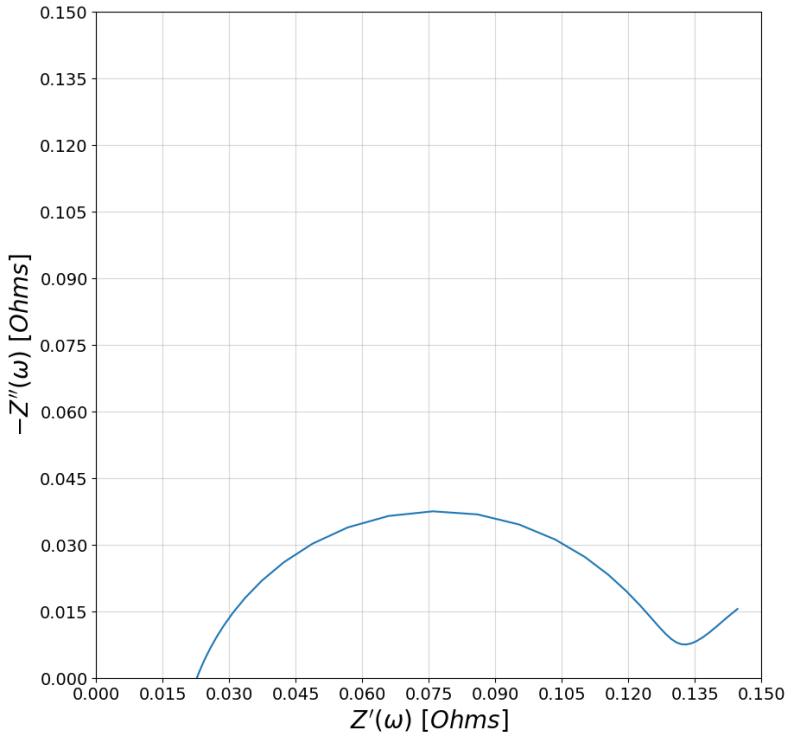

Figure 4.2: Nyquist plot of the equivalent circuit with the average values from all the uncycled batteries

This initial characterization of the battery's impedance will be important for analysing the final EIS data of the aged cells. In order to further this battery's characterization, and to identify the so far unknown electrode materials, a study on incremental capacity is proposed. As the peaks in this curve equate to the several redox reactions happening within the cathode and anode while charging and discharging the device, specific materials will have different peak patterns, as these reactions occur at specific electrochemical potentials. Thus, with an analysis of previous literature on sodium-ion batteries, we can compare at which voltage levels these reactions occur in our material and determine which material better fits our values. This is extremely important for the analysis of the degradation mechanisms, as these vary in many ways with the inner composition of the battery. As many of the defined protocols change the way the batteries are cycled, either with different current profiles or different voltage limits, to better ensure that the observed values were correct this characterization was limited to more conservative protocols: 1CR, CR/5, FC1C, FCC/2 and DS. All the batteries cycled in these protocols were used to obtain these values. Using the *scipy.signal* package in *python*, we were able to sort the peaks in differential capacity and their respective potentials, saving the relevant ones to a file. Much like the case for the EIS, the average of the values in the file was calculated, obtaining the following values:

1st Charging Peak	2nd Charging Peak	1st Discharging Dip	2nd Discharging Dip
$3.05V$	$3.50V$	$2.72V$	$3.25V$

Table 4.2: Average potential values of the charging peaks and the discharging dips (1st represents the most intense peak/dip)

Searching through literature on SIBs, an electrode material combination is identified in the study [62]. In this study, a sodium-ion cell is developed with an iron based prussian blue cathode ($Na_{2-x}FeFe(CN)_6$) and a commercial hard carbon anode. This research included cyclic voltammetry curves which have the same general shape as the differential capacity curves, as their peaks and dips also correspond to the redox reactions in the battery. As we can observe in figure 4.3, the positions of the peaks and dips are very similar, and the voltage values positions are identical.

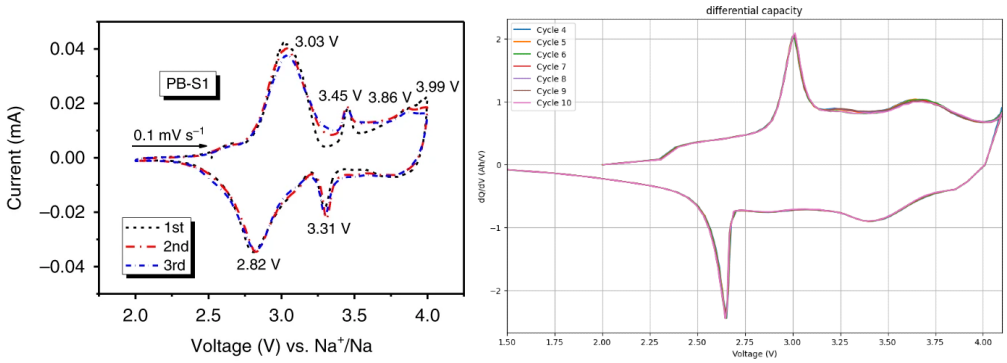

Figure 4.3: Left: From [62], cyclic voltammetry curve of the PB-HC battery ; Right: dQ/dV plots from the first 10 cycles of the 1CR-2 cell

The first charging peak, with the highest intensity, is a result of the reduction reaction of high spin Fe^{2+} connected with N atoms, with the smaller peaks being caused by smaller spin Fe^{2+} connected to C atoms. With complex structures like prussian blue, the insertion and removal of sodium ions often cause phase changes of the whole crystal structure. In our case, studies found that iron based PBs Have two main structure modes: rhombohedral and cubic. [63]

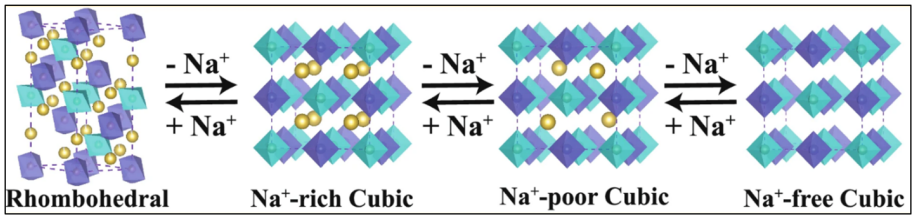

Figure 4.4: From [63]: Schematic representation of the phase transitions accompanying sodium insertion/removal (represented in yellow)

The rhombohedral structure is better suited to accommodate for a larger amount of Na ions, thus it is the phase of the fully charged cathode. The Na-rich, Na-poor and Na-free cubic structures change in parameter and volume, but the overall lattice organization is maintained. The shift from rhombohedral to cubic should be associated with the first charge peak and discharge peak, as they correspond to the high spin iron reactions. High spin Fe2+ has a radius around 22% larger and 52% bigger volume, thus their redox reactions lead to higher vacancies and variation within the cathode, causing a phase shift [64]. As for the anode, hard carbon is a very common material used in SIBs, so the interactions with sodium ions is already a subject under study. It is composed of several disordered graphene-like layered structures with spacious interlayer distances and defects, ideal to store Na ions. These ions are also stored in micro and nanopores present within and in the surface of HC particles. The dips observed in the differential capacity curve are related to the battery discharge and to the ion removal through redox reactions in the anode. The dip present at higher potential is related to the defects and interlayer spaces, as these present a stronger bind to Na, while the 1st, higher intensity dip relates to the nanopore bound ions. [35]

4.2. C-Rate Protocols

The first step to properly analyse the aging and degradation of these cells is to observe the overall capacity tendency. This will indicate to us if the protocol was more conservative or destructive, if it led to sudden spikes or losses in capacity and how they fared against relative cycling profiles. Much like the case in the experimental methods protocol section, we will divide this analysis in 4 groups, to better understand how each specific factor in a protocol may affect the cell aging. The first group has protocols relating to the charge/discharge C-rate, in simple constant current cycles within the full working voltage of the battery. As we can see, the overall better performance seems to be from the 1CR protocol, cycled at 1C C-rate, maintaining most of the cells' capacity through the cycles at above 80%, for cells 2 and 3, and around 70% for cell 1. The other profiles follow simple downward, linear trends, with the 3CR protocol having one battery with a sudden drop at around 170 cycles, the only in this group to drop below 50% capacity retention. The batteries cycled at 2CR also seem to lose more capacity when compared to the 1CR protocol, ending their cycling around 50%-60%, with the CR/5 protocol obtaining remarkably similar results to 1CR. These two seem to be the better protocols for the battery's health, but with the added caveat that cycles under the CR/5 protocol last 5 times longer than the 1CR protocol.

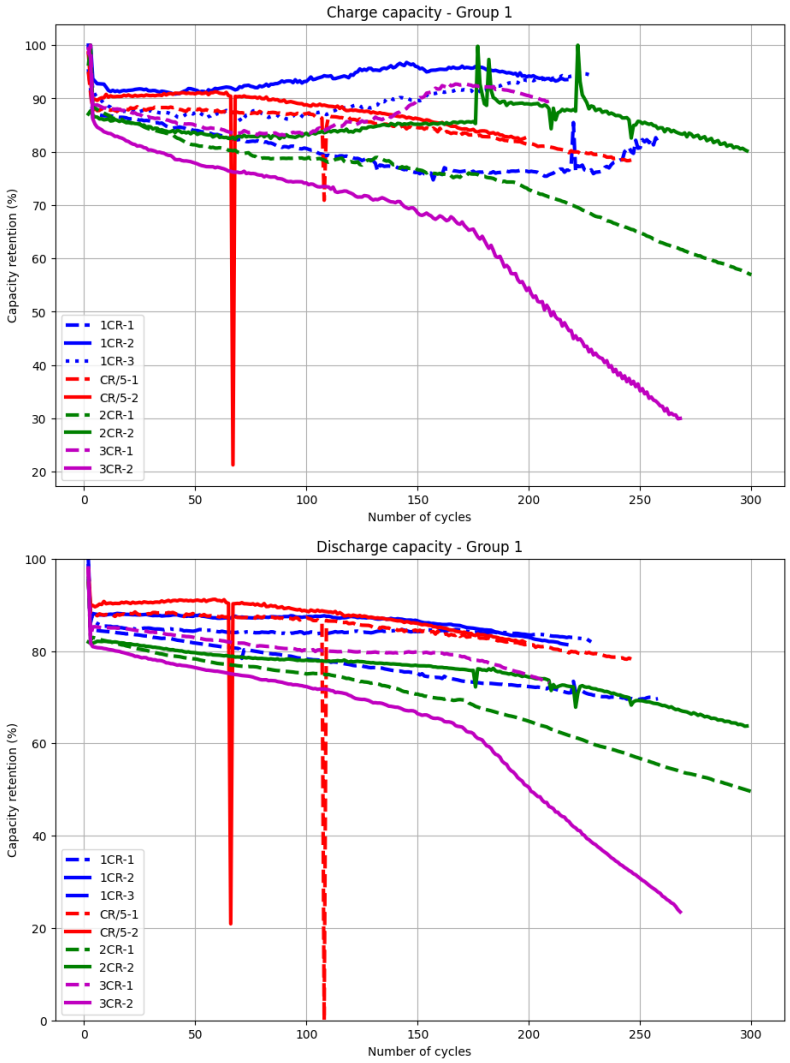

Figure 4.5: Comparison of capacity retention among protocols with varying C-rate (on top charging capacity, on bottom discharging capacity)

The sudden, single point drops present in the CR/5 cells are from a sudden error in the battery tester, forcing the cycling to stop, which we later resumed once the problem was solved.

As for the analysis of the electrode degradation, using the differential capacity curves at several key cycles in each protocol, we can see an immediate effect on the peak position. The peaks seem to shift towards higher potentials with higher C-rate, as is to be expected with how the batteries tend to reach these higher potentials at faster speeds. The overall peak amplitude is also affected by this, as the lower C-rates see a stronger peak intensity at every cycle. This, in part, is caused by the longer cycle duration, leading to near full completion of the reduction reactions respective to the peaks, and aligns with the observable lower capacity in the higher C-rate cells when compared to the CR/5 protocol[65].

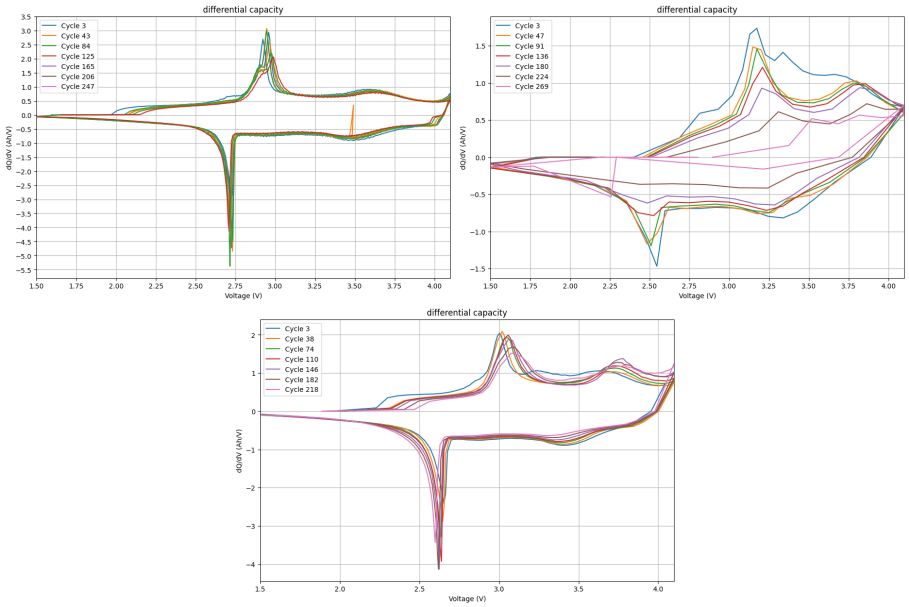

Figure 4.6: Differential capacity plots for batteries CR/5-1 (top-left), 3CR-2 (top-right) and 1CR-2 (bottom)

With the cyclic aging in each battery, we observe the peak intensity diminishing and the peak position shift slightly to the right with the increasing cycles. This peak intensity fade effect is greater in the cathode than in the anode, as the charging peaks change considerably more than the discharge dips, leading to the conclusion that most degradation is within the cathode. The dimming of the discharge dips is mostly due to the formation of the SEI layer, as both the intensity fade and the layer growth should be more prominent in the 2CR protocol.

4.3. SoC Window Protocols

In the second group, the factor in focus was the SoC range used in the charge/discharge cycles, done by limiting the working voltage used in these protocols. As a result, only a portion of the total battery capacity was used in these cases, with 80% for SCup and SCdown and 60% for SClim. Even taking this into account, the SoC limiting protocols have very clear drops in capacity retention beyond their limits. The worst case for this seems to happen under the SCup profile, as both cells completely lose all working capacity before reaching 100 cycles. SCdown has a similar drop in cell 1, but at a much later cycle (225), while the other cell seems to follow a very identical aging trend as 1CR-1, but with lower overall capacity, given the circumstances of their cycling profiles. SClim does not present any sudden drops, but at the end of the procedure the capacity retention is nearing 10%.

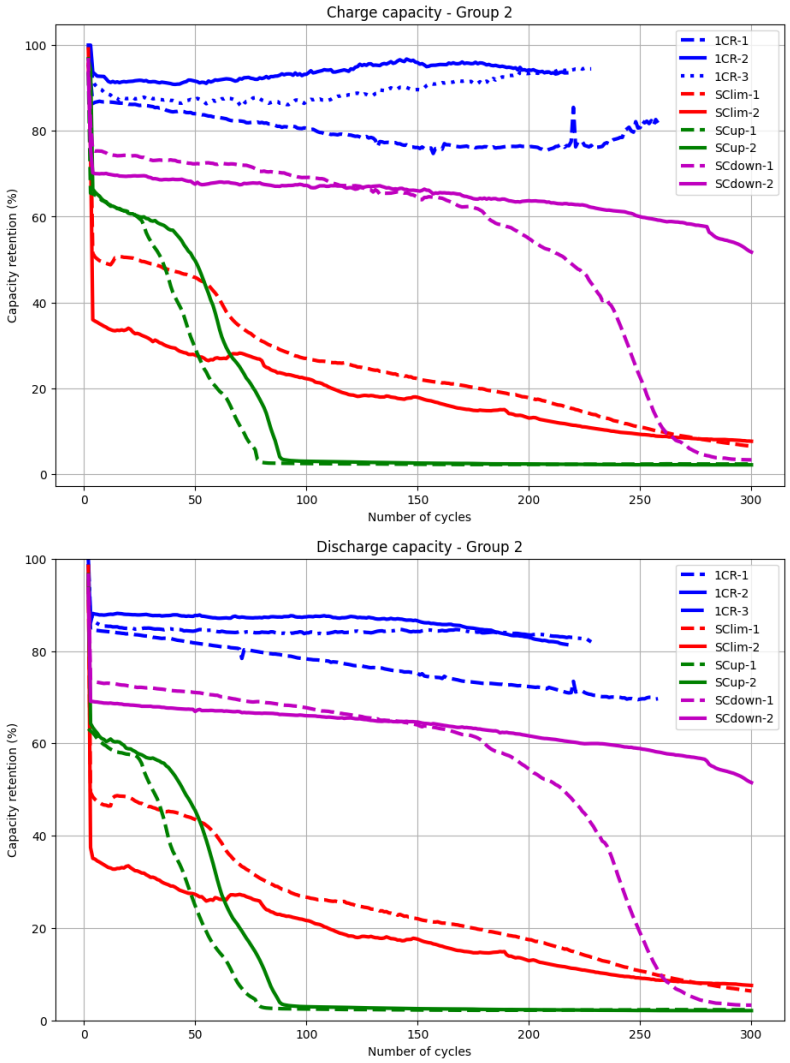

Figure 4.7: Comparison of capacity retention among protocols with varying pulse profiles (on top charge, on bottom discharge capacity)

As for the differential capacity curves, these protocols are particularly interesting as, given their structure limiting the working voltage limits of the battery, not all reactions occur as expected. For example, in our case, the biggest discharging dip (2.7 V) takes place near the voltage defined for 20% SoC (2.6 V), thus this reaction is often incomplete or missing in the SClim and SCup protocols. As these peaks represent the redox reactions that cause the ionic and electron conductivity between the electrodes, these reactions are not being completed, leading to a lower electron flow in the external circuit, thus a lower ion flow within the battery. The reason SCup presents much higher impedance over the other protocols is a combination of SEI formation and cathode deterioration. SEI growth and thickening is accentuated in higher potential, and this profile reaches the upper limit of the total working voltage of the battery. Not only does a bigger SEI increase the impedance

of the cell, but it also consumes some of the few sodium ions in circulation during this protocol.

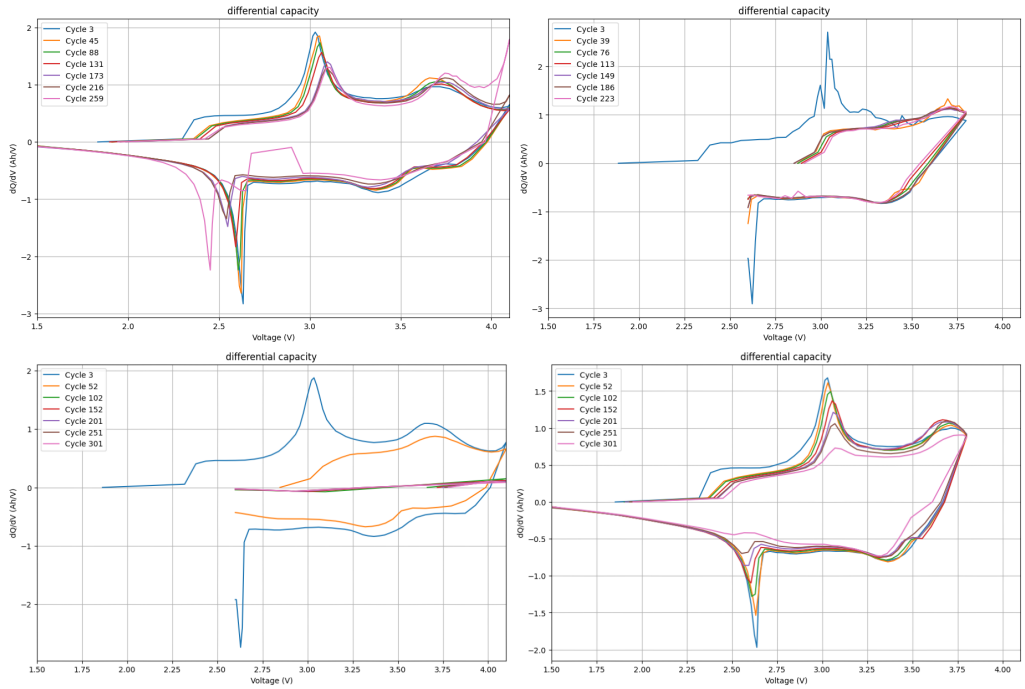

Figure 4.8: Differential capacity plots for batteries 1CR-1 (top-left), SClim-1 (top-right), SCup-2 (bottom-left), SCdown-2 (bottom-right)

As the voltage limits for SCdown are more distant in relation to the more important redox reactions in the electrodes, and being 0.3 V higher than the second charging peak, both of these reactions are observed in these cycles. As these curves are representing the differential capacity, the graph area below the plotted line represents the capacity of the cell, and as there is a big portion of area missing above the cutoff voltage (3.8 V), there is once again a significant portion of the sodium ions that are not being removed from the electrodes. This incites a snowballing loss of capacity, as without fully completing all the redox reactions the sodium ions being unused will be accumulated in the electrodes, causing the diminishing amplitude of the dQ/dV curves observed for this protocol. In the SCdown-1 cell this led to a drop and eventual end of life, but before it followed a very similar trend to SCdown-2. [63]

As our batteries present a prussian blue cathode that suffers phase shifts during the charging and discharging of the ions in its lattice, these incomplete redox reactions contribute to the degradation of its very lattice. For the cases with incomplete high spin Fe reactions, this damage is much more aggressive and sooner in the cycle life, as these reactions are accompanied by the bigger shift in structure from rhombohedral to cubic. As these redox

shifts don't fully occur, there is a possibility that this shift doesn't take place in these protocols, creating stress in the cathode as it is in a much less suitable phase to receive the Na ions. While not as aggressively, as the high spin redox reaction seems to be present, the case for SCdown isn't much different, albeit much less aggressive. The shifts between the several cubic phases the electrode goes through are much smaller, but still cause strain and conflicts if they do not properly accompany the ion movement within the cell.

4.4. Pulse Profile Protocols

For group 3, the protocols tackled the shape of the charge/discharge current applied to the batteries. In this instance all these protocols followed the reference 1CR in terms of capacity retention, as all of them finished with more than 70% of total capacity. This indicates these profiles are much more conservative on cell degradation than the previous groups. The stepped nature of the capacity retention, with several plateaus and almost fixed values showing, is a result of the protocols themselves, as given the way they are structured certain cycles will have more or less pulses depending on their speed in reaching maximum voltage or capacity.

The pulse protocols provide faster charging/discharging times, cutting it by about 25 minutes in PCR and around 15 minutes in PCC, when compared to the 125minutes it takes in 1CR, without compromising capacity retention. Due to the nature of the pulse profile in these protocols, and how our battery tester saves data, the differential capacity plots cannot be fully obtained in a readable state, as each pulse registers several very disperse values of dQ/dV in each step, summing up to around 30 pulses per charge/discharge.

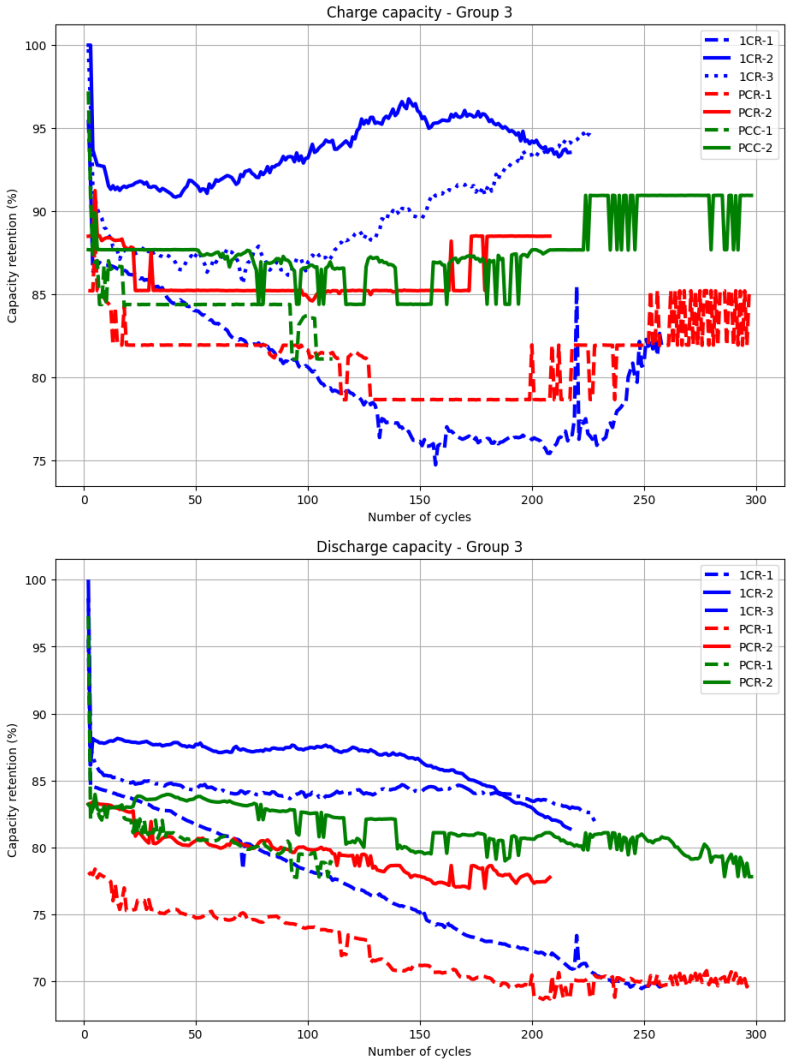

Figure 4.9: Comparison of capacity retention among pulse profile protocols (on top charge, on bottom discharge capacity)

4.5. CC-CV and Asymmettrical Protocols

As for the fourth group, for a better understanding of the curves it was split into two subgroups, one with the 1CR protocol as reference and another with the protocol DS as reference. In this first subgroup, the influence of the constant voltage step when cycling is tested. For the FC1C and FCC/2 protocols, this step is present in both the charge and the discharge, as for the DS cells, it is only present in the charge. Except for FCC/2, these protocols have massive and sudden drops in capacity retention, with FC1C-1 resisting almost 250 cycles before dropping harshly to the point of activation safety mechanisms in the battery tester. Until this drop, the cell had a very similar behaviour to 1CR-3. As for the FCC/2 protocol, the batteries stopped early from exceeding the charge capacity safety limits. The constant voltage step seems to have a major destructive effect on degradation.

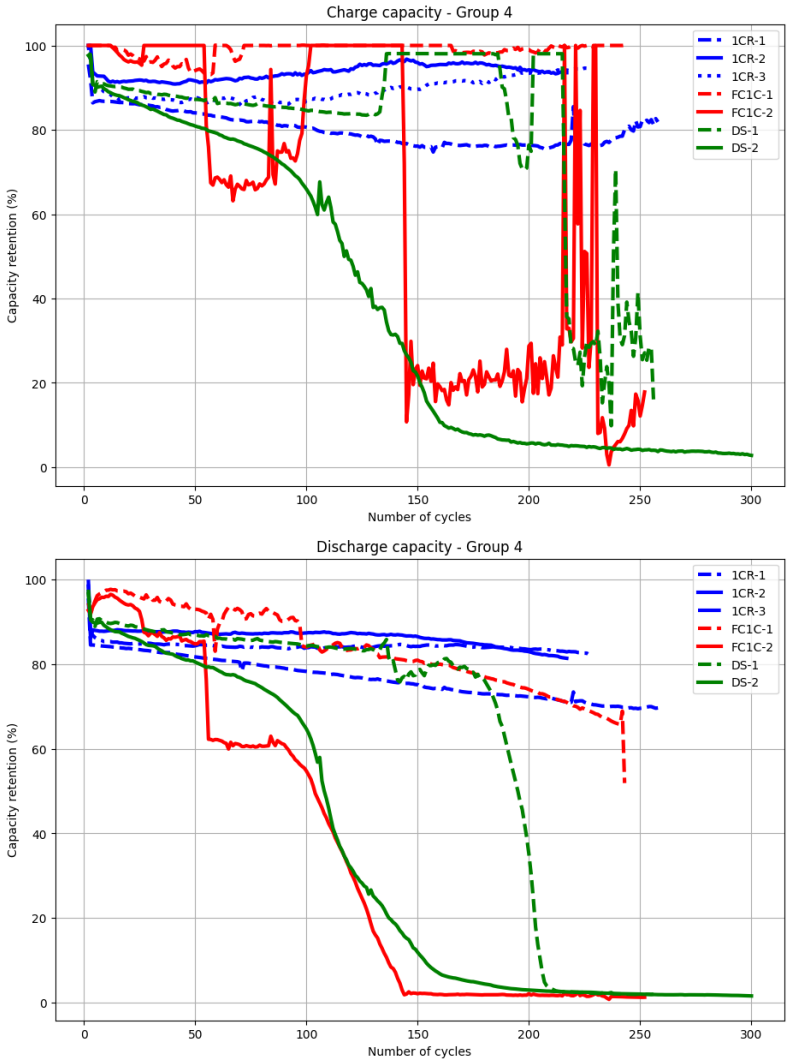

Figure 4.10: Comparison of capacity retention among CC-CV protocols (on top charge, on bottom discharge capacity)

As for the subgroup with DS as a reference, the protocols FastDC and StepDC were included for comparison. Both have the CV step present only in the charging phase. In all of these protocols we can observe total failure and end of life for all cells, leading to the conclusion that the complete CCCV charge has some correlation to very aggressive degradation.

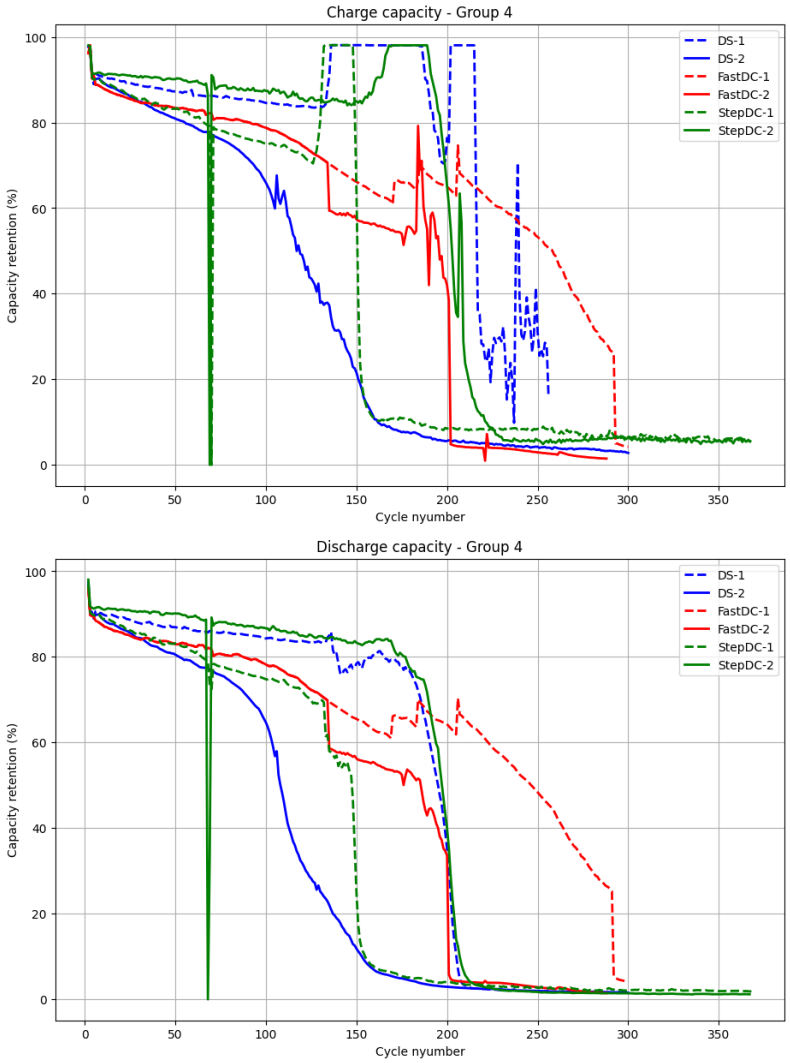

Figure 4.11: Comparison of capacity retention among asymmetrical protocols (on top charge, on bottom discharge capacity)

To properly evaluate the full extent of the damage done to the electrodes, the differential capacity curves are once again a useful tool. As we can see in the figure below, all these protocols had their redox reaction peaks and dips diminish and shifting slightly to the right throughout the cycles, until the cell reaches full collapse.

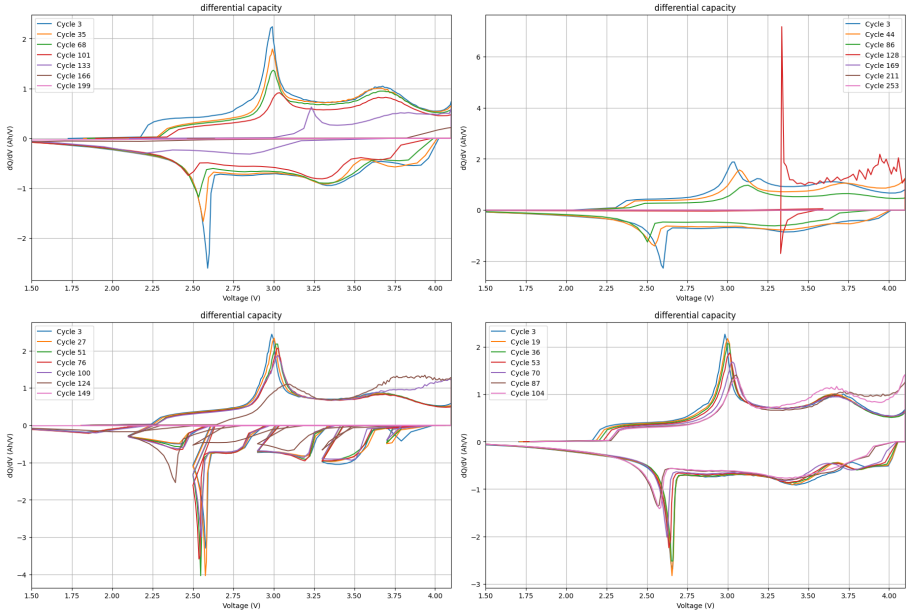

Figure 4.12: Differential capacity plots for batteries DS-1 (top-left), FastDC-2 (top-right), StepDC-2 (bottom-left), FCC/2-2 (bottom-right)

As these protocols only have the CV step in common, it should be the root cause of this extreme capacity loss. The constant voltage step is held at the end of the charge at high potential values, which is also an extremely active zone for ion mobility and side reactions within the battery. In these protocols some later cycles had a small capacity recuperation, also visible in the differential capacity at higher potential, that originated in partial dissolution of SEI layer, releasing Na ions that were previously considered consumed. On the structural side of the electrodes, experiencing a full charge/discharge, and therefore full insertion/removal of the intercalated ions, may lead to irreversible phase shift. The rhombohedral structure of the prussian blue, when filled with sodium with a nonstop constant voltage, may become extremely stressed, as sodium ions are large and introduce lack of balance in the lattice.

4.6. Post-Mortem Analysis

Due to unknown circumstances, some batteries were fully discharged and damaged to the point where it was impossible to perform the final EIS in them. 1CR-2, 1CR-3 and all the batteries with the 3CR, FC1C and FCC/2 protocols were all affected. When trying to safely charge these cells up to better potential values to try and EIS, even with small currents of 0.001 C-rate, the voltage would shoot up beyond the safety limits into the 6V range. This means a highly elevated internal impedance and resistance is present, but

without being able to work with the device in acceptable voltage values we cannot perform the final EIS test.

As most impedance curves in the cycled batteries are quite different from one another, even in similar protocols, there is very little interest in averaging all the fitted circuits to obtain a simulated EIS standard for all cells. Observing the general final EIS Nyquist plots, it is noticeable that some have a complete second semicircle in the charge transfer region, thus a second parallel split with a resistor and a CPE should be included in the equivalent circuit. Some batteries show a small shoulder shift at higher frequency region, thus leading to incorporating a third CPE right before the parallel circuit split. The resulting equivalent circuit is shown in Figure 4.13. As these final plots vary between all the protocols and even between cells with similar protocols, we can't define specific average values transversal and applicable to all the batteries.

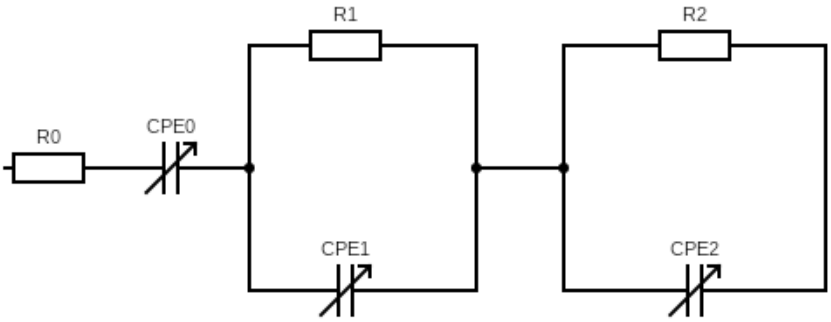

Figure 4.13: Equivalent circuit fitted in general to all post-mortem EIS

To fittingly compare all the final Nyquist plots between each other, the reference curve will be defined as the fitted circuit presented in figure 4.1 D, with the average values of the circuit elements.

4.6.1 Group 1 - C-Rate Variation

As we can observe in the EIS, after cycling the ionic conductivity area of the Nyquist plot forms a second semicircle, indicating an increase in interfacial impedance within the cells. As was the case with the capacity retention, the protocols 1CR and CR/5 seem to present curves much closer to the initial fit when compared to 2CR, which shows much higher values of impedance and, in the cell 2CR-1, an increase in the initial resistance. This indicates that a major degradation mechanism present in these batteries is the SEI, as the elongated semicircle along with a second one represent slower kinetics, mostly

from passivating interfacial layers like the SEI. Thus, we can conclude that the formation and thickening of this layer increases with higher C-rates. This effect originates from the faster diffusion rates of the ions, which the electrodes cannot always keep up with, leading to aggravated polarization and boosting side reaction, such as SEI growth. Although not measured, the higher currents and higher resistance should lead to higher internal temperatures, further facilitating electrolyte dissolution. [66]

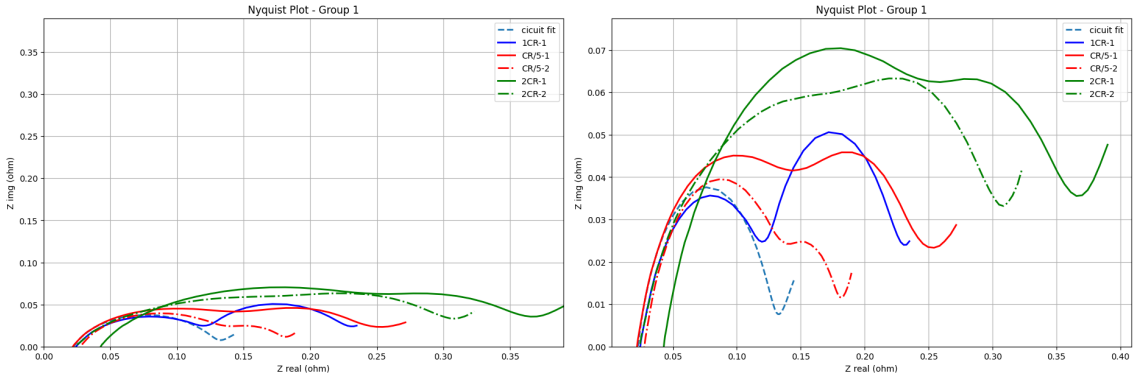

Figure 4.14: Comparison between Nyquist plots for the Group 1 batteries (square plot with equal axis on the left, more zoomed in on the right)

4.6.2 Group 2 - SoC Windows

In the second group, we were able to perform the final EIS on all of the batteries, thus providing deeper knowledge on the effects of all the protocols. As noted in the previous section, these protocols proved all to be much more destructive than the reference 1CR protocol, as most of the cells reached total failure with an end of life below 10% capacity retention.

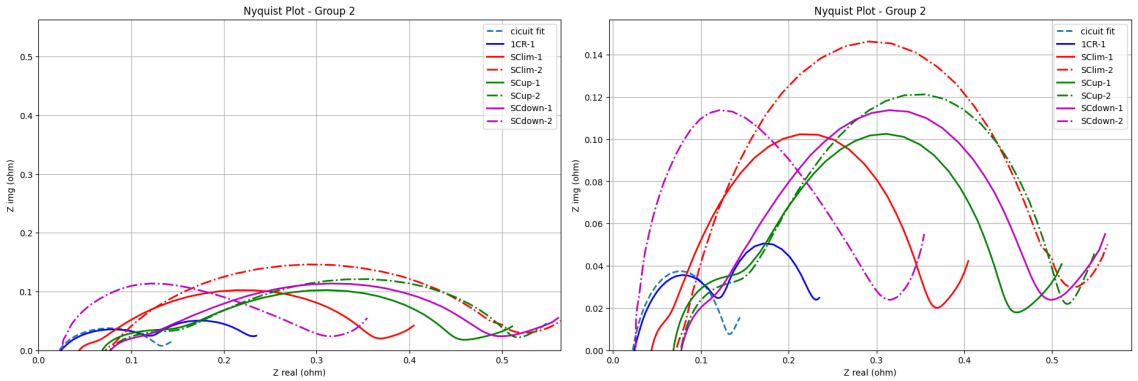

Figure 4.15: Comparison between Nyquist plots for the Group 2 batteries (square plot with equal axis on the left, more zoomed in on the right)

Unlike the C-rate protocols, these cells did not form a second semicircle after cycling, instead their impedance in the only semicircle increased much more, reaching the 100 mΩ

range. The overall shape of the Nyquist plots is identical between these protocols, with initial resistance also increased in every cell that reached end of life, and a small shoulder shift present at high frequencies, in this case equating to the interfacial impedance, mostly driven up by the SEI layer. These shoulders are much more pronounced in the SCup protocol, this is due to the SEI layer having bigger growth in high potential values, and therefore higher SoC. [67]

4.6.3 Group 3 - Pulse Profiles

In the third group, the cell PCC-1 is a particular case as external electrical issues caused an early stop in the protocol, but in the data we do have it showed a very identical behaviour to PCC-2. The overall EIS plots of this group resemble the graph for the first group, with a second semicircle forming in the ionic conductivity region and very little change to the initial resistance. This is in agreement with the capacity retention results, confirming the conservative nature of these profiles. The bigger impedance in the semicircles when compared to 1CR protocol are a cause of bigger SEI growth in the higher C-rate steps of the pulses, at either 2C (PCR) or 1.5C (PCC).

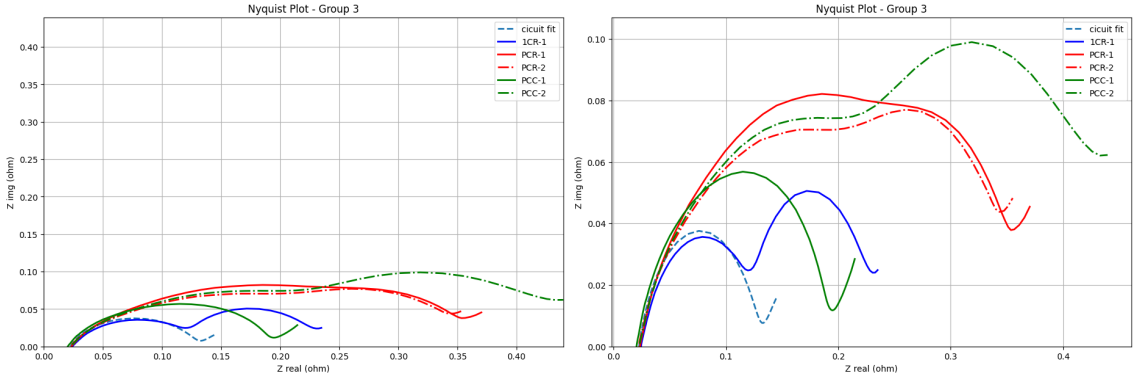

Figure 4.16: Comparison between Nyquist plots for the Group 3 batteries (square plot with equal axis on the left, more zoomed in on the right)

4.6.4 Group 4 - CC-CV and Asymmetrical protocols

For the batteries in group 4, we were unable to perform a final EIS on the cells cycled with the FC1C and FCC/2 protocols. As for the DS, StepDC and FastDC protocols, they present the biggest impedance of all the tested batteries in this study, up to 3.5 Ω in the more extreme case (StepDC-2). All the plots seem to have at least a hint at a second semicircle indicating serious interfacial issue. Taking this into account with the sheer magnitude of the impedance, there must be intense structural degradation in the electrodes, with possible cracking and breaking of the connections between components. As

these protocols include at least one constant voltage step, the cells spend a lot more time in higher potentials, which, as already discussed, promote bigger growth in the SEI layer and other side reactions, causing a rapid consumption of sodium ion inventory.

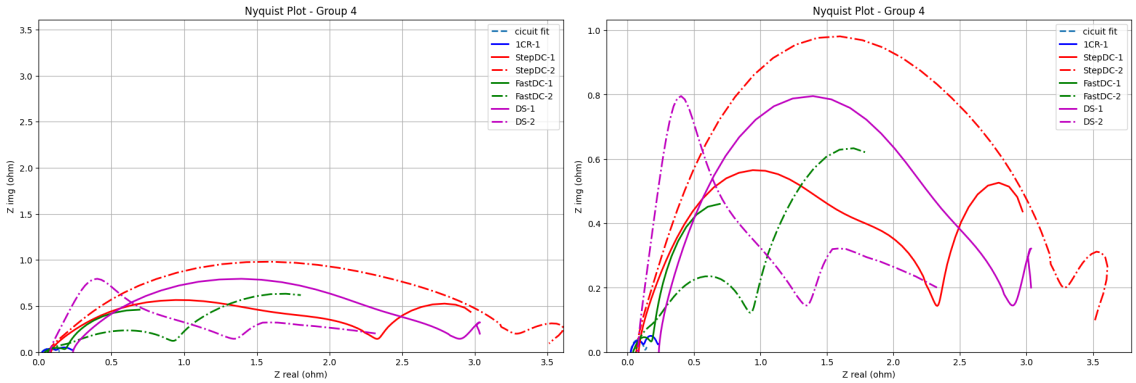

Figure 4.17: Comparison between Nyquist plots for the Group 4 batteries (square plot with equal axis on the left, more zoomed in on the right)

4.7. Limitations of the study

As an aging work this study is, naturally, limited to time constraints. Some batteries with more conservative protocols had a capacity retention in higher percentages above 70%, thus never reached total degradation with more challenging and impactful degradation mechanisms. A larger time window would also allow for an extra comparative aging reference with calendar aged cells, which would provide extra insight into the true effect of the specific factors of the protocols. The number of cells is also somewhat limiting, as with more available units more protocols could have been tested and their reproducibility could have been tested further, possibly avoiding problems like lost data or batteries that could not have the final EIS tests done.

5. Conclusions and Future Work

5.1. Main Findings

This thesis set out with the goal to evaluate the impact of varying charge/discharge profiles on the cyclic aging of SIBs, experimentally testing several protocols with different C-rate, Soc windows, pulse and CC-CV profiles. The specific degradation mechanisms present in these batteries are identified by comparing and analysing their cycling metrics and their changes through the cycles, identifying factors that contribute to aging and major challenges in this technology.

Beginning with an initial characterization of the batteries prior to cycling, in order to better understand how the degradation mechanisms evolve within them, an equivalent circuit to fit the average EIS Nyquist curve was created. Using differential capacity analysis, the curve's peaks and dips were identified to determine the electrode materials of our objects of work. Comparing with literature lead to the conclusion that these cells have an iron-based prussian blue cathode ($Na_{2-x}FeFe(CN)_6$) and a hard carbon anode.

Several protocols were developed and split into groups for an easier analysis of specific charge/discharge profiles. The first group proved how the overall capacity retention of a cell greatly reduces with higher current C-rate, caused by a bigger SEI growth in those conditions, still exhibiting some stability. The second group, focused on the SoC windows, revealed a major flaw in the PBA materials. These cathodes, while the battery is cycling, will change between several phases depending on the amount of sodium ions filling vacant spaces. As these phase changes accompany the cathode's redox reactions, limiting SoC limits these reactions, and the phase transitions become incomplete, resulting in sodium trapping and major structural damage. Hence it was discovered that using a wide, full 100% SoC range for cycling is preferable. As for the third group, the pulse charging profiles were found to be significantly faster than a standard CC charge (around 20% for PCR and 12% for PCC) without compromising capacity retention, as their results were comparable to the reference cases of the first group. In the final group, the constant voltage step was linked to a bigger capacity loss as a result of the full charge/discharge causing higher stress and possible irreversible phase transition in the electrodes. These steps also lead to more time spent at higher voltage states, which enforces a bigger SEI growth, impacting the impedance and resistance of these cells.

This study managed to connect several charge/discharge variables to the specific degradation mechanisms of SIBs, identifying SEI growth and cathode phase transitions and stress as the main challenges they face, with certain protocols such as simple CC C-rate and pulse profiles helping avoid these degradation mechanisms.

5.2. Future Perspectives

In the future, bigger studies with more protocols and cycled units would help better understand the degradation with each factor, even expanding to variables not explored in this study like temperature. With a bigger dataset it would also be possible to develop a machine learning predictive algorithm, to simulate battery degradation with several protocols. Several post-mortem characterization techniques, such as XRD and SEM, could be applied to gain deeper knowledge on the changes occurring in the electrodes. This deeper knowledge could lead to research on better electrode materials or additives that could tackle these degradation mechanisms, improving the state of the art for sodium-ion batteries and improving this promising technology.

References

[1] L. Zhao, T. Zhang, W. Li, T. Li, L. Zhang, X. Zhang, and Z. Wang, “Engineering of sodium-ion batteries: Opportunities and challenges,” *Engineering*, vol. 24, pp. 172–183, 2023. [Online]. Available: https://www.sciencedirect.com/science/article/pii/S2095809922003630 [Cited on page 1.]

[2] Z. Yang, J. Zhang, M. C. Kintner-Meyer, X. Lu, D. Choi, J. P. Lemmon, and J. Liu, “Electrochemical energy storage for green grid,” *Chem Rev*, vol. 111, no. 5, p. 3577–613, 2011, yang, Zhenguo Zhang, Jianlu Kintner-Meyer, Michael C W Lu, Xiaochuan Choi, Daiwon Lemmon, John P Liu, Jun eng 2011/03/08 Chem Rev. 2011 May 11;111(5):3577-613. doi: 10.1021/cr100290v. Epub 2011 Mar 4. [Online]. Available: https://www.ncbi.nlm.nih.gov/pubmed/21375330 [Cited on page 1.]

[3] M. D. Slater, D. Kim, E. Lee, and C. S. Johnson, “Sodium-ion batteries,” *Advanced Functional Materials*, vol. 23, no. 8, pp. 947–958, 2013. [Online]. Available: https://advanced.onlinelibrary.wiley.com/doi/abs/10.1002/adfm.201200691 [Cited on page 1.]

[4] T. Hosaka, K. Kubota, A. S. Hameed, and S. Komaba, “Research development on k-ion batteries,” *Chem Rev*, vol. 120, no. 14, p. 6358–6466, 2020, hosaka, Tomooki Kubota, Kei Hameed, A Shahul Komaba, Shinichi eng 2020/01/16 Chem Rev. 2020 Jul 22;120(14):6358-6466. doi: 10.1021/acs.chemrev.9b00463. Epub 2020 Jan 15. [Online]. Available: https://www.ncbi.nlm.nih.gov/pubmed/31939297 [Cited on page 1.]

[5] S. Yang, F. Zhang, H. Ding, P. He, and H. Zhou, “Lithium metal extraction from seawater,” *Joule*, vol. 2, no. 9, p. 1648–1651, 2018. [Online]. Available: https://doi.org/10.1016/j.joule.2018.07.006 [Cited on page 1.]

[6] F. Calvão, C. E. A. Mcdonald, and M. Bolay, “Cobalt mining and the corporate outsourcing of responsibility in the democratic republic of congo,” *The Extractive Industries and Society*, vol. 8, no. 4, p. 100884, 2021. [Online]. Available: https://www.sciencedirect.com/science/article/pii/S2214790X21000290 [Cited on page 1.]

[7] P. Yadav, V. Shelke, A. Patrike, and M. Shelke, “Sodium-based batteries: development, commercialization journey and new emerging chemistries,” *Oxford Open Materials Science*, vol. 3, no. 1, p. itac019, Dec. 2022, _eprint: https://academic.oup.com/ooms/article-pdf/3/1/itac019/48770894/itac019.pdf. [Online]. Available: https://doi.org/10.1093/oxfmat/itac019 [Cited on page 2.]

[8] M. Li, “Elevating the practical application of sodium-ion batteries through advanced characterization studies on cathodes,” *Energies*, vol. 16, no. 24, 2023. [Online]. Available: https://www.mdpi.com/1996-1073/16/24/8004 [Cited on page 2.]

[9] A. G. Olabi, Q. Abbas, P. A. Shinde, and M. A. Abdelkareem, “Rechargeable batteries: Technological advancement, challenges, current and emerging applications,” *Energy*, vol. 266, p. 126408, 2023. [Online]. Available: https://www.sciencedirect.com/science/article/pii/S0360544222032947 [Cited on page 4.]

[10] G. Ozsin, “An overview of sodium-ion batteries as next-generation sustainable electrochemical devices beyond the traditional lithium-ion framework,” *Turk J Chem*, vol. 49, no. 1, p. 1–28, 2025, ozsin, Gamzenur eng Review Turkey 2025/03/19 Turk J Chem. 2024 Sep 17;49(1):1-28. doi: 10.55730/1300-0527.3707. eCollection 2025. [Online]. Available: https://www.ncbi.nlm.nih.gov/pubmed/40104108 [Cited on pages viii, 5, and 7.]

[11] N. Yabuuchi, K. Kubota, M. Dahbi, and S. Komaba, “Research development on sodium-ion batteries,” *Chem Rev*, vol. 114, no. 23, p. 11636–82, 2014, yabuuchi, Naoaki Kubota, Kei Dahbi, Mouad Komaba, Shinichi eng 2014/11/13 Chem Rev. 2014 Dec 10;114(23):11636-82. doi: 10.1021/cr500192f. Epub 2014 Nov 12. [Online]. Available: https://www.ncbi.nlm.nih.gov/pubmed/25390643 [Cited on pages 5 and 6.]

[12] M. M. Doeff, Y. Ma, S. J. Visco, and L. C. De Jonghe, “Electrochemical insertion of sodium into carbon,” *Journal of The Electrochemical Society*, vol. 140, no. 12, p. L169, dec 1993. [Online]. Available: https://doi.org/10.1149/1.2221153 [Cited on page 5.]

[13] L. W. Shacklette, T. R. Jow, and L. Townsend, “Rechargeable electrodes from sodium cobalt bronzes,” *Journal of The Electrochemical Society*, vol. 135, no. 11,

p. 2669, nov 1988. [Online]. Available: https://doi.org/10.1149/1.2095407 [Cited on page 5.]

[14] K. Chayambuka, G. Mulder, D. L. Danilov, and P. H. L. Notten, “Sodium-ion battery materials and electrochemical properties reviewed,” *Advanced Energy Materials*, vol. 8, no. 16, p. 1800079, 2018. [Online]. Available: https://advanced.onlinelibrary.wiley.com/doi/abs/10.1002/aenm.201800079 [Cited on page 5.]

[15] J. Peng, W. Zhang, Q. Liu, J. Wang, S. Chou, H. Liu, and S. Dou, “Prussian blue analogues for sodium-ion batteries: Past, present, and future,” *Adv Mater*, vol. 34, no. 15, p. e2108384, 2022, peng, Jian Zhang, Wang Liu, Qiannan Wang, Jiazhao Chou, Shulei Liu, Huakun Dou, Shixue eng DP180101453/Australian Research Council/ G00849/Australian Renewable Energy Agency/ International Centre for Diffraction Data/ Ludo Frevel Crystallography Scholarship/ Postgraduate Research Award/ Review Germany 2021/12/18 Adv Mater. 2022 Apr;34(15):e2108384. doi: 10.1002/adma.202108384. Epub 2022 Feb 24. [Online]. Available: https://www.ncbi.nlm.nih.gov/pubmed/34918850 [Cited on page 6.]

[16] Q. Ni, Y. Bai, F. Wu, and C. Wu, “Polyanion-type electrode materials for sodium-ion batteries,” *Adv Sci (Weinh)*, vol. 4, no. 3, p. 1600275, 2017, ni, Qiao Bai, Ying Wu, Feng Wu, Chuan eng Review Germany 2017/03/24 Adv Sci (Weinh). 2017 Jan 25;4(3):1600275. doi: 10.1002/advs.201600275. eCollection 2017 Mar. [Online]. Available: https://www.ncbi.nlm.nih.gov/pubmed/28331782 [Cited on page 7.]

[17] W. Zhang, F. Zhang, F. Ming, and H. N. Alshareef, “Sodium-ion battery anodes: Status and future trends,” *EnergyChem*, vol. 1, no. 2, p. 100012, 2019. [Online]. Available: https://www.sciencedirect.com/science/article/pii/S2589778019300156 [Cited on page 7.]

[18] J. Meng, G. Jia, H. Yang, and M. Wang, “Recent advances for sei of hard carbon anode in sodium-ion batteries: A mini review,” *Front Chem*, vol. 10, p. 986541, 2022, meng, Jiaqi Jia, Guofeng Yang, Hongjun Wang, Min eng Review Switzerland 2022/10/08 Front Chem. 2022 Sep 20;10:986541. doi: 10.3389/fchem.2022.986541. eCollection 2022. [Online]. Available: https://www.ncbi.nlm.nih.gov/pubmed/36204151 [Cited on page 7.]

[19] P. Phogat, S. Dey, and M. Wan, “Comprehensive review of sodium-ion batteries: Principles, materials, performance, challenges, and future perspectives,” *Materials Science and Engineering: B*, vol. 312, p. 117870, 2025. [Online]. Available: https://www.sciencedirect.com/science/article/pii/S0921510724006998 [Cited on page 7.]

[20] X. Lei, F. Xie, J. Wang, and C. Zhang, “A review of lithium-ion battery state of health and remaining useful life estimation methods based on bibliometric analysis,” *Journal of Traffic and Transportation Engineering (English Edition)*, vol. 11, no. 6, pp. 1420–1446, 2024. [Online]. Available: https://www.sciencedirect.com/science/article/pii/S2095756424001193 [Cited on page 8.]

[21] J. S. Edge, S. O’Kane, R. Prosser, N. D. Kirkaldy, A. N. Patel, A. Hales, A. Ghosh, W. Ai, J. Chen, J. Yang, S. Li, M. C. Pang, L. Bravo Diaz, A. Tomaszewska, M. W. Marzook, K. N. Radhakrishnan, H. Wang, Y. Patel, B. Wu, and G. J. Offer, “Lithium ion battery degradation: what you need to know,” *Phys Chem Chem Phys*, vol. 23, no. 14, p. 8200–8221, 2021, edge, Jacqueline S O’Kane, Simon Prosser, Ryan Kirkaldy, Niall D Patel, Anisha N Hales, Alastair Ghosh, Abir Ai, Weilong Chen, Jingyi Yang, Jiang Li, Shen Pang, Mei-Chin Bravo Diaz, Laura Tomaszewska, Anna Marzook, M Waseem Radhakrishnan, Karthik N Wang, Huizhi Patel, Yatish Wu, Billy Offer, Gregory J eng England 2021/04/21 Phys Chem Chem Phys. 2021 Apr 14;23(14):8200-8221. doi: 10.1039/d1cp00359c. Epub 2021 Mar 26. [Online]. Available: https://www.ncbi.nlm.nih.gov/pubmed/33875989 [Cited on page 8.]

[22] S. Wang, Y. Fan, D.-I. Stroe, C. Fernandez, C. Yu, W. Cao, and Z. Chen, “Chapter 1 - lithium-ion battery characteristics and applications,” in *Battery System Modeling*, S. Wang, Y. Fan, D.-I. Stroe, C. Fernandez, C. Yu, W. Cao, and Z. Chen, Eds. Elsevier, 2021, pp. 1–46. [Online]. Available: https://www.sciencedirect.com/science/article/pii/B9780323904728000032 [Cited on page 8.]

[23] D. Anseán, V. M. García, M. González, C. Blanco-Viejo, J. C. Viera, Y. F. Pulido, and L. Sánchez, “Lithium-ion battery degradation indicators via incremental capacity analysis,” *IEEE Transactions on Industry Applications*, vol. 55, no. 3, pp. 2992–3002, 2019. [Online]. Available: https://doi.org/10.1109/TIA.2019.2891213 [Cited on page 9.]

[24] J. Zhu, M. S. Dewi Darma, M. Knapp, D. R. Sørensen, M. Heere, Q. Fang, X. Wang, H. Dai, L. Mereacre, A. Senyshyn, X. Wei, and H. Ehrenberg, “Investigation

of lithium-ion battery degradation mechanisms by combining differential voltage analysis and alternating current impedance," *Journal of Power Sources*, vol. 448, p. 227575, 2020. [Online]. Available: https://www.sciencedirect.com/science/article/pii/S037877531931568X [Cited on page 9.]

[25] B. Kishore, L. Chen, C. E. J. Dancer, and E. Kendrick, "Electrochemical formation protocols for maximising the life-time of a sodium ion battery," *Chem Commun (Camb)*, vol. 56, no. 85, p. 12925–12928, 2020, kishore, Brij Chen, Lin Dancer, Claire E J Kendrick, Emma eng England 2020/09/26 Chem Commun (Camb). 2020 Oct 27;56(85):12925-12928. doi: 10.1039/d0cc05673a. [Online]. Available: https://www.ncbi.nlm.nih.gov/pubmed/32974624 [Cited on page 9.]

[26] V. A. Agubra and J. W. Fergus, "The formation and stability of the solid electrolyte interface on the graphite anode," *Journal of Power Sources*, vol. 268, pp. 153–162, 2014. [Online]. Available: https://www.sciencedirect.com/science/article/pii/S0378775314008775 [Cited on page 10.]

[27] S. S. Madani, Y. Shabeer, F. Allard, M. Fowler, C. Ziebert, Z. Wang, S. Panchal, H. Chaoui, S. Mekhilef, S. X. Dou, K. See, and K. Khalilpour, "A comprehensive review on lithium-ion battery lifetime prediction and aging mechanism analysis," *Batteries*, vol. 11, no. 4, 2025. [Online]. Available: https://www.mdpi.com/2313-0105/11/4/127 [Cited on page 10.]

[28] B. Sun, P. Xiong, U. Maitra, D. Langsdorf, K. Yan, C. Wang, J. Janek, D. Schröder, and G. Wang, "Design strategies to enable the efficient use of sodium metal anodes in high-energy batteries," *Advanced Materials*, vol. 32, no. 18, p. 1903891, 2020. [Online]. Available: https://advanced.onlinelibrary.wiley.com/doi/abs/10.1002/adma.201903891 [Cited on pages viii and 10.]

[29] L. F. Pfeiffer, Y. Li, M. Mundszinger, J. Geisler, C. Pfeifer, D. Mikhailova, A. Omar, V. Baran, J. Biskupek, U. Kaiser, P. Adelhelm, M. Wohlfahrt-Mehrens, S. Passerini, and P. Axmann, "Origin of aging of a p2-naxmn3/4ni1/4o2 cathode active material for sodium-ion batteries," *Chemistry of Materials*, vol. 35, no. 19, pp. 8065–8080, 2023. [Online]. Available: https://doi.org/10.1021/acs.chemmater.3c01499 [Cited on page 10.]

[30] L. A. Ma, A. Buckel, A. Hofmann, L. Nyholm, and R. Younesi, "Fundamental understanding and quantification of capacity losses involving the negative electrode

in sodium-ion batteries," *Adv Sci (Weinh)*, vol. 11, no. 6, p. e2306771, 2024, ma, Le Anh Buckel, Alexander Hofmann, Andreas Nyholm, Leif Younesi, Reza eng The Swedish Energy Agency/ Deutsche Forschungsgemeinschaft/ 2016-01257/Svenska Forskningsradet Formas/ Germany 2023/12/07 Adv Sci (Weinh). 2024 Feb;11(6):e2306771. doi: 10.1002/advs.202306771. Epub 2023 Dec 7. [Online]. Available: https://www.ncbi.nlm.nih.gov/pubmed/38059817 [Cited on page 10.]

[31] Y. Zheng, H. Xie, J. Li, K. S. Hui, Z. Yu, H. Xu, D. A. Dinh, Z. Ye, C. Zha, and K. N. Hui, "Insights into the jahn-teller effect in layered oxide cathode materials for potassium-ion batteries," *Advanced Energy Materials*, vol. 14, no. 14, p. 2400461, 2024. [Online]. Available: https://advanced.onlinelibrary.wiley.com/doi/abs/10.1002/aenm.202400461 [Cited on page 11.]

[32] Y. Li, G. Liu, J. Che, L. Chen, X. Wang, G. Wang, L. Lei, J. Hou, S. Li, J. Wang, Y. Xu, and Y. Zhao, "Review on layered oxide cathodes for sodium-ion batteries: Degradation mechanisms, modification strategies, and applications," *Interdisciplinary Materials*, vol. 4, no. 1, pp. 24–51, 2025. [Online]. Available: https://onlinelibrary.wiley.com/doi/abs/10.1002/idm2.12213 [Cited on page 11.]

[33] Y. Xiao, J. Xiao, H. Zhao, J. Li, G. Zhang, D. Zhang, X. Guo, H. Gao, Y. Wang, J. Chen, G. Wang, and H. Liu, "Prussian blue analogues for sodium-ion battery cathodes: A review of mechanistic insights, current challenges, and future pathways," *Small*, vol. 20, no. 35, p. e2401957, 2024, xiao, Yang Xiao, Jun Zhao, Hangkai Li, Jiayi Zhang, Guilai Zhang, Dingyi Guo, Xin Gao, Hong Wang, Yong Chen, Jun Wang, Guoxiu Liu, Hao eng SKLASS 2021-04/Shanghai Key Laboratory of Advanced Ferrometallurgy, Shanghai University/ 22010500400/Science and Technology Commission of Shanghai Municipality/ 23PJ1402800/Shanghai Pujiang Program/ DP220101290/Australian Research Council/ Review Germany 2024/04/29 Small. 2024 Aug;20(35):e2401957. doi: 10.1002/smll.202401957. Epub 2024 Apr 29. [Online]. Available: https://www.ncbi.nlm.nih.gov/pubmed/38682730 [Cited on page 11.]

[34] J. J. Marie, R. A. House, G. J. Rees, A. W. Robertson, M. Jenkins, J. Chen, S. Agrestini, M. Garcia-Fernandez, K. J. Zhou, and P. G. Bruce, "Trapped o(2) and the origin of voltage fade in layered li-rich cathodes," *Nat Mater*, vol. 23, no. 6, p. 818–825, 2024, marie, John-Joseph House,

Robert A Rees, Gregory J Robertson, Alex W Jenkins, Max Chen, Jun Agrestini, Stefano Garcia-Fernandez, Mirian Zhou, Ke-Jin Bruce, Peter G eng EP/R00661X/1/RCUK | Engineering and Physical Sciences Research Council (EPSRC)/ EP/S019367/1/RCUK | Engineering and Physical Sciences Research Council (EPSRC)/ EP/R010145/1/RCUK | Engineering and Physical Sciences Research Council (EPSRC)/ EP/L019469/1/RCUK | Engineering and Physical Sciences Research Council (EPSRC)/ FIRG016/RCUK | Engineering and Physical Sciences Research Council (EPSRC)/ England 2024/03/02 Nat Mater. 2024 Jun;23(6):818-825. doi: 10.1038/s41563-024-01833-z. Epub 2024 Mar 1. [Online]. Available: https://www.ncbi.nlm.nih.gov/pubmed/38429520 [Cited on page 11.]

[35] R. Qiu, D. Ma, H. Zheng, M. Liu, J. Cai, W. Yan, and J. Zhang, “Performance degradation mechanisms and mitigation strategies of hard carbon anode and solid electrolyte interface for sodium-ion battery,” *Nano Energy*, vol. 128, p. 109920, 2024. [Online]. Available: https://www.sciencedirect.com/science/article/pii/S2211285524006682 [Cited on pages 11 and 30.]

[36] P. Harks, F. Mulder, and P. Notten, “In situ methods for li-ion battery research: A review of recent developments,” *Journal of Power Sources*, vol. 288, pp. 92–105, 2015. [Online]. Available: https://www.sciencedirect.com/science/article/pii/S0378775315007417 [Cited on page 11.]

[37] P. M. Attia, A. Bills, F. Brosa Planella, P. Dechent, G. dos Reis, M. Dubarry, P. Gasper, R. Gilchrist, S. Greenbank, D. Howey, O. Liu, E. Khoo, Y. Preger, A. Soni, S. Sripad, A. G. Stefanopoulou, and V. Sulzer, “Review—“knees” in lithium-ion battery aging trajectories,” *Journal of The Electrochemical Society*, vol. 169, no. 6, p. 060517, jun 2022. [Online]. Available: https://doi.org/10.1149/1945-7111/ac6d13 [Cited on page 12.]

[38] A. C. Lazanas and M. I. Prodromidis, “Electrochemical impedance spectroscopy-a tutorial,” *ACS Meas Sci Au*, vol. 3, no. 3, p. 162–193, 2023, lazanas, Alexandros Ch Prodromidis, Mamas I eng Review 2023/06/26 ACS Meas Sci Au. 2023 Mar 8;3(3):162-193. doi: 10.1021/acsmeasuresciau.2c00070. eCollection 2023 Jun 21. [Online]. Available: https://www.ncbi.nlm.nih.gov/pubmed/37360038 [Cited on page 12.]

[39] L. A. Middlemiss, A. J. Rennie, R. Sayers, and A. R. West, “Characterisation of batteries by electrochemical impedance spectroscopy,” *Energy Reports*, vol. 6,

pp. 232–241, 2020, 4th Annual CDT Conference in Energy Storage & Its Applications. [Online]. Available: https://www.sciencedirect.com/science/article/pii/S2352484720303103 [Cited on pages viii, 12, and 13.]

[40] N. O. Laschuk, E. B. Easton, and O. V. Zenkina, "Reducing the resistance for the use of electrochemical impedance spectroscopy analysis in materials chemistry," *RSC Adv*, vol. 11, no. 45, p. 27925–27936, 2021, laschuk, Nadia O Easton, E Bradley Zenkina, Olena V eng Review England 2022/04/29 RSC Adv. 2021 Aug 18;11(45):27925-27936. doi: 10.1039/d1ra03785d. eCollection 2021 Aug 16. [Online]. Available: https://www.ncbi.nlm.nih.gov/pubmed/35480766 [Cited on page 13.]

[41] K. Amine, C. Chen, J. Liu, M. Hammond, A. Jansen, D. Dees, I. Bloom, D. Vissers, and G. Henriksen, "Factors responsible for impedance rise in high power lithium ion batteries," *Journal of Power Sources*, vol. 97-98, pp. 684–687, 2001, proceedings of the 10th International Meeting on Lithium Batteries. [Online]. Available: https://www.sciencedirect.com/science/article/pii/S0378775301007017 [Cited on page 13.]

[42] R. Guo, L. Lu, M. Ouyang, and X. Feng, "Mechanism of the entire overdischarge process and overdischarge-induced internal short circuit in lithium-ion batteries," *Sci Rep*, vol. 6, p. 30248, 2016, guo, Rui Lu, Languang Ouyang, Minggao Feng, Xuning eng Research Support, Non-U.S. Gov't England 2016/07/23 Sci Rep. 2016 Jul 22;6:30248. doi: 10.1038/srep30248. [Online]. Available: https://www.ncbi.nlm.nih.gov/pubmed/27444934 [Cited on page 14.]

[43] D. DiLecce, V. Marangon, M. Isaacs, R. Palgrave, P. R. Shearing, and J. Hassoun, "Degradation of layered oxide cathode in a sodium battery: A detailed investigation by x-ray tomography at the nanoscale," *Small Methods*, vol. 5, no. 10, p. e2100596, 2021, diLecce, Daniele Marangon, Vittorio Isaacs, Mark Palgrave, Robert Shearing, Paul R Hassoun, Jusef eng Fondo di Ateneo per la Ricerca Locale/ Accordo di Collaborazione Quadro 2015/ Department of Chemical and Pharmaceutical Sciences/ EP/K005030/1/EPSRC/ CiET1718/59/EPSRC/ EP/S003053/1/EPSRC/ HarwellXPS/EPSRC National Facility for XPS/ Cardiff University/ Accordo/Sapienza Universita di Roma/ di/Sapienza Universita di Roma/ Collaborazione/Sapienza Universita di Roma/ Quadro/Sapienza Universita di Roma/ 2015/Sapienza Universita di Roma/

PR16195/Engineering and Physical Sciences Research Council/ FAR 2020/Universita degli Studi di Ferrara/ Research Support, Non-U.S. Gov't Germany 2021/12/21 Small Methods. 2021 Oct;5(10):e2100596. doi: 10.1002/smtd.202100596. Epub 2021 Aug 21. [Online]. Available: https://www.ncbi.nlm.nih.gov/pubmed/34927950 [Cited on page 14.]

[44] Y. Preger, H. M. Barkholtz, A. Fresquez, D. L. Campbell, B. W. Juba, J. Romàn-Kustas, S. R. Ferreira, and B. Chalamala, "Degradation of commercial lithium-ion cells as a function of chemistry and cycling conditions," *Journal of The Electrochemical Society*, vol. 167, no. 12, p. 120532, sep 2020. [Online]. Available: https://doi.org/10.1149/1945-7111/abae37 [Cited on page 14.]

[45] G. Ning, B. Haran, and B. N. Popov, "Capacity fade study of lithium-ion batteries cycled at high discharge rates," *Journal of Power Sources*, vol. 117, no. 1, pp. 160–169, 2003. [Online]. Available: https://www.sciencedirect.com/science/article/pii/S0378775303000296 [Cited on page 15.]

[46] E. Wikner and T. Thiringer, "Extending battery lifetime by avoiding high soc," *Applied Sciences*, vol. 8, no. 10, 2018. [Online]. Available: https://www.mdpi.com/2076-3417/8/10/1825 [Cited on page 15.]

[47] N. Kirkaldy, M. A. Samieian, G. J. Offer, M. Marinescu, and Y. Patel, "Lithium-ion battery degradation: Comprehensive cycle ageing data and analysis for commercial 21700 cells," *Journal of Power Sources*, vol. 603, p. 234185, 2024. [Online]. Available: https://www.sciencedirect.com/science/article/pii/S0378775324001368 [Cited on page 15.]

[48] F. An, R. Zhang, Z. Wei, and P. Li, "Multi-stage constant-current charging protocol for a high-energy-density pouch cell based on a 622ncm/graphite system," *RSC Adv*, vol. 9, no. 37, p. 21498–21506, 2019, an, Fuqiang Zhang, Rui Wei, Zhiguo Li, Ping eng England 2019/07/10 RSC Adv. 2019 Jul 10;9(37):21498-21506. doi: 10.1039/c9ra03629f. eCollection 2019 Jul 5. [Online]. Available: https://www.ncbi.nlm.nih.gov/pubmed/35521330 [Cited on page 15.]

[49] J. Liu and X. Wang, "Experimental study of the effect of different pulse charging patterns on lithium-ion battery charging," *Journal of Power Sources*, vol. 610, p. 234700, 2024. [Online]. Available: https://www.sciencedirect.com/science/article/pii/S0378775324006529 [Cited on pages viii, 15, 16, and 23.]

[50] D. R. Rajagopalan Kannan and M. H. Weatherspoon, “The effect of pulse charging on commercial lithium nickel cobalt oxide (nmc) cathode lithium-ion batteries,” *Journal of Power Sources*, vol. 479, p. 229085, 2020. [Online]. Available: https://www.sciencedirect.com/science/article/pii/S037877532031380X [Cited on page 16.]

[51] J. M. Amanor-Boadu, A. Guiseppi-Elie, and E. Sánchez-Sinencio, “The impact of pulse charging parameters on the life cycle of lithium-ion polymer batteries,” *Energies*, vol. 11, no. 8, 2018. [Online]. Available: https://www.mdpi.com/1996-1073/11/8/2162 [Cited on page 16.]

[52] D. Juarez-Robles, A. A. Vyas, C. Fear, J. A. Jeevarajan, and P. P. Mukherjee, “Overcharge and aging analytics of li-ion cells,” *Journal of The Electrochemical Society*, vol. 167, no. 9, p. 090547, jun 2020. [Online]. Available: https: //doi.org/10.1149/1945-7111/ab9569 [Cited on page 17.]

[53] R. Wang, X. Zhou, Y. Wang, Y. Xiao, Z. Shi, Y. Liu, and T. Zhang, “Degradation analysis of lithium-ion batteries under ultrahigh-rate discharge profile,” *Applied Energy*, vol. 376, p. 124241, 2024. [Online]. Available: https://www.sciencedirect. com/science/article/pii/S0306261924016246 [Cited on page 17.]

[54] L. Nguyen, P. S. Camacho, J. Fondard, D. Carlier, L. Croguennec, M. Palacin, A. Ponrouch, C. Courrèges, R. Dedryvère, K. Trad, C. Jordy, S. Genies, Y. Reynier, and L. Simonin, “First 18650-format na-ion cells aging investigation: A degradation mechanism study,” *Journal of Power Sources*, vol. 529, p. 231253, 2022. [Online]. Available: https://www.sciencedirect.com/science/article/pii/S0378775322002701 [Cited on pages 17 and 22.]

[55] E. Irujo, A. Berrueta, P. Sanchis, and A. Ursúa, “Experimental characterization and aging analysis of commercial 18650 sodium-ion cells,” in *2024 International Conference on Renewable Energies and Smart Technologies (REST)*, 2024, pp. 1–5. [Online]. Available: https://ieeexplore.ieee.org/document/10645381 [Cited on page 18.]

[56] W. Li, H. Xie, S. Lin, Y. Qin, J. Zeng, P. Zhang, and J. Zhao, “Insights on the degradation mechanism of 7 ah sodium ion batteries at different aging modes,” *Journal of Power Sources*, vol. 639, p. 236635, 2025. [Online].

Available: https://www.sciencedirect.com/science/article/pii/S0378775325004719 [Cited on page 18.]

[57] H. Zhang, Y. Gao, X. Liu, L. Zhou, J. Li, Y. Xiao, J. Peng, J. Wang, and S.-L. Chou, “Long-cycle-life cathode materials for sodium-ion batteries toward large-scale energy storage systems,” *Advanced Energy Materials*, vol. 13, no. 23, p. 2300149, 2023. [Online]. Available: https://advanced.onlinelibrary.wiley.com/doi/abs/10.1002/aenm.202300149 [Cited on page 19.]

[58] S. Lochab, S. Bharathraj, K. S. Mayya, P. Barpanda, and S. P. Adiga, “Unveiling the degradation mechanism of sodium ion batteries based on na4fe3(po4)2p2o7 cathode and hard carbon anode suggests anode particle size reduction for cycling stability,” *Batteries & Supercaps*, vol. 7, no. 8, p. e202400025, 2024. [Online]. Available: https://chemistry-europe.onlinelibrary.wiley.com/doi/abs/10.1002/batt.202400025 [Cited on page 19.]

[59] S. Jenu, A. Hentunen, J. Haavisto, and M. Pihlatie, “State of health estimation of cycle aged large format lithium-ion cells based on partial charging,” *Journal of Energy Storage*, vol. 46, p. 103855, 2022. [Online]. Available: https://www.sciencedirect.com/science/article/pii/S2352152X21015243 [Cited on page 23.]

[60] Y. Gao, J. Jiang, C. Zhang, W. Zhang, and Y. Jiang, “Aging mechanisms under different state-of-charge ranges and the multi-indicators system of state-of-health for lithium-ion battery with li(nimnco)o2 cathode,” *Journal of Power Sources*, vol. 400, pp. 641–651, 2018. [Online]. Available: https://www.sciencedirect.com/science/article/pii/S0378775318307262 [Cited on page 23.]

[61] W. Wheeler, Y. Bultel, P. Venet, and A. Sari, “An ageing study of twenty 18650 lithium-ion graphite/lfp cells in first and second life use,” *Sci Data*, vol. 12, no. 1, p. 392, 2025, wheeler, William Bultel, Yann Venet, Pascal Sari, Ali eng CIFRE 2018/1625/Association Nationale de la Recherche et de la Technologie (National Association for Research and Technology)/ England 2025/03/07 Sci Data. 2025 Mar 6;12(1):392. doi: 10.1038/s41597-025-04712-7. [Online]. Available: https://www.ncbi.nlm.nih.gov/pubmed/40050317 [Cited on page 24.]

[62] W. Wang, Y. Gang, Z. Hu, Z. Yan, W. Li, Y. Li, Q. F. Gu, Z. Wang, S. L. Chou, H. K. Liu, and S. X. Dou, “Reversible structural evolution of sodium-rich rhombohedral prussian blue for sodium-ion batteries,” *Nat Commun*, vol. 11, no. 1,

p. 980, 2020, wang, Wanlin Gang, Yong Hu, Zhe Yan, Zichao Li, Weijie Li, Yongcheng Gu, Qin-Fen Wang, Zhixing Chou, Shu-Lei Liu, Hua-Kun Dou, Shi-Xue eng 201606370024/China Scholarship Council (CSC)/ England 2020/02/23 Nat Commun. 2020 Feb 20;11(1):980. doi: 10.1038/s41467-020-14444-4. [Online]. Available: https://www.ncbi.nlm.nih.gov/pubmed/32080172 [Cited on pages viii and 29.]

[63] H. Zhang, J. Li, J. Liu, Y. Gao, Y. Fan, X. Liu, C. Guo, H. Liu, X. Chen, X. Wu, Y. Liu, Q. Gu, L. Li, J. Wang, and S. L. Chou, "Understanding capacity fading from structural degradation in prussian blue analogues for wide-temperature sodium-ion cylindrical battery," *Nat Commun*, vol. 16, no. 1, p. 2520, 2025, zhang, Hang Li, Jiayang Liu, Jinhang Gao, Yun Fan, Yameng Liu, Xiaohao Guo, Chaofei Liu, Haoxuan Chen, Xiudong Wu, Xingqiao Liu, Yang Gu, Qinfen Li, Li Wang, Jiazhao Chou, Shu-Lei eng England 2025/03/14 Nat Commun. 2025 Mar 13;16(1):2520. doi: 10.1038/s41467-025-57663-3. [Online]. Available: https://www.ncbi.nlm.nih.gov/pubmed/40082420 [Cited on pages viii, 29, and 34.]

[64] J.-F. Lin, S. Speziale, Z. Mao, and H. Marquardt, "Effects of the Electronic Spin Transitions of Iron in Lower Mantle Minerals: Implications for Deep Mantle Geophysics and Geochemistry," *Reviews of Geophysics*, vol. 51, no. 2, pp. 244–275, Apr. 2013. [Cited on page 30.]

[65] J. Z. Olson, C. M. López, and E. J. F. Dickinson, "Differential analysis of galvanostatic cycle data from li-ion batteries: Interpretative insights and graphical heuristics," *Chemistry of Materials*, vol. 35, no. 4, pp. 1487–1513, 2023. [Online]. Available: https://doi.org/10.1021/acs.chemmater.2c01976 [Cited on page 31.]

[66] Y. Yang, L. Chen, L. Yang, X. Du, and Y. Yang, "Capacity fade characteristics of lithium iron phosphate cell during dynamic cycle," *Energy*, vol. 206, p. 118155, 2020. [Online]. Available: https://www.sciencedirect.com/science/article/pii/S0360544220312627 [Cited on page 41.]

[67] L. Zhao, S. I. Costa, Y. Chen, J. R. Fitzpatrick, A. J. Naylor, O. Kolosov, and N. Tapia-Ruiz, "A comparative study of solid electrolyte interphase evolution in ether and ester-based electrolytes for Na-ion batteries," *PRX Energy*, vol. 4, p. 033002, Jul 2025. [Online]. Available: https://link.aps.org/doi/10.1103/jfvb-wp5w [Cited on page 42.]